



UNIVERSITÀ
DEGLI STUDI
FIRENZE

FLORE

Repository istituzionale dell'Università degli Studi di Firenze

A New Metric for Measuring the Security of an Environment: The Secrecy Pressure

Questa è la Versione finale referata (Post print/Accepted manuscript) della seguente pubblicazione:

Original Citation:

A New Metric for Measuring the Security of an Environment: The Secrecy Pressure / Mucchi, L.; Ronga, L.; Zhou, X.; Huang, K.; Chen, Y.; Wang, R.. - In: IEEE TRANSACTIONS ON WIRELESS COMMUNICATIONS. - ISSN 1536-1276. - STAMPA. - 16:(2017), pp. 3416-3430. [10.1109/TWC.2017.2682245]

Availability:

The webpage <https://hdl.handle.net/2158/1079632> of the repository was last updated on 2017-12-10T10:19:34Z

Published version:

DOI: 10.1109/TWC.2017.2682245

Terms of use:

Open Access

La pubblicazione è resa disponibile sotto le norme e i termini della licenza di deposito, secondo quanto stabilito dalla Policy per l'accesso aperto dell'Università degli Studi di Firenze (<https://www.sba.unifi.it/upload/policy-oa-2016-1.pdf>)

Publisher copyright claim:

Conformità alle politiche dell'editore / Compliance to publisher's policies

Questa versione della pubblicazione è conforme a quanto richiesto dalle politiche dell'editore in materia di copyright.

This version of the publication conforms to the publisher's copyright policies.

La data sopra indicata si riferisce all'ultimo aggiornamento della scheda del Repository FloRe - The above-mentioned date refers to the last update of the record in the Institutional Repository FloRe

(Article begins on next page)

A New Metric for Measuring the Security of an Environment: The Secrecy Pressure

Lorenzo Mucchi, *Senior Member, IEEE*, Luca Ronga, *Senior Member, IEEE*, Xiangyun Zhou, *Member, IEEE*, Kaibin Huang, *Senior Member, IEEE*, Yifan Chen, *Senior Member, IEEE*, and Rui Wang

Abstract—Information-theoretical approaches can ensure security, regardless of the computational power of the attackers. Requirements for the application of this theory are: 1) assuring an advantage over the eavesdropper quality of reception and 2) knowing where the eavesdropper is. The traditional metrics are the secrecy capacity or outage, which are both related to the quality of the legitimate link against the eavesdropper link. Our goal is to define a new metric, which is the characteristic of the security of the surface/environment where the legitimate link is immersed, regardless of the position of the eavesdropping node. The contribution of this paper is twofold: 1) a general framework for the derivation of the secrecy capacity of a surface, which considers all the parameters that influence the secrecy capacity and 2) the definition of a new metric to measure the secrecy of a surface: the secrecy pressure. The metric can be also visualized as a secrecy map, analogously to weather forecast. Different application scenarios are shown: from “forbidden zone” to Gaussian mobility model for the eavesdropper. Moreover, the secrecy outage probability of a surface is derived. This additional metric can measure, which is the secrecy rate supportable by the specific environment.

Index Terms—Physical-layer security, secrecy pressure, secrecy capacity, secrecy outage, security of wireless communications.

I. INTRODUCTION

IN WIRELESS networks, transmission between legitimate nodes can easily be intercepted by an eavesdropper due to the broadcast nature of the wireless medium. This makes

Manuscript received September 12, 2016; revised January 20, 2017; accepted February 28, 2017. The work of X. Zhou was supported by the Australian Research Council’s Discovery Projects under Grant DP150103905. The work of Y. Chen was supported by the Guangdong Natural Science Funds under Grant 2016A030313640. The associate editor coordinating the review of this paper and approving it for publication was M. ElKashlan.

L. Mucchi is with the Department of Information Engineering, University of Florence, I-50139 Firenze, Italy (e-mail: lorenzo.mucchi@unifi.it).

L. Ronga is with the National Inter-universities Consortium on Telecommunications, University of Firenze research Unit, I-50139 Firenze, Italy (e-mail: luca.ronga@cnit.it).

X. Zhou is with the Research School of Engineering, Australian National University, Canberra, ACT 0200, Australia (e-mail: xiangyun.zhou@anu.edu.au).

K. Huang is with the Department of Electrical and Electronic Engineering, The University of Hong Kong, Hong Kong (e-mail: huangkb@iee.org).

Y. Chen is with the Faculty of Science and Engineering, The University of Waikato, Hamilton 3240, New Zealand, also with the Faculty of Computing and Mathematical Sciences, The University of Waikato, Hamilton 3240, New Zealand, and also with the Department of Electrical and Electronic Engineering, Southern University of Science and Technology, Shenzhen 518055, China (e-mail: yifan.chen@waikato.ac.nz).

R. Wang is with the Department of Electrical and Electronic Engineering, South University of Science and Technology of China, Shenzhen 518055, China (e-mail: wang.r@sustc.edu.cn).

Color versions of one or more of the figures in this paper are available online at <http://ieeexplore.ieee.org>.

Digital Object Identifier 10.1109/TWC.2017.2682245

wireless transmissions highly vulnerable to eavesdropping attacks. Existing communications systems typically adopt cryptographic techniques in order to achieve confidential transmission, to prevent an eavesdropper from interpreting data transmission between legitimate users.

It is known that encrypted transmission is not perfectly secure, since the cipher text can still be decrypted by an eavesdropper through a brute-force attack, an exhaustive search of the encryption key into the cipher text.

To this end, physical-layer security is an emerging alternative paradigm to protect wireless communications against eavesdropping attacks, including brute-force attacks. In fact, the security of cryptographic techniques is implicitly set into the practical assumption that the attacker does not have enough computational power to hack the cipher text in a reasonable amount of time. Thus, security of encryption algorithm cannot be measured exactly. On the contrary, information-theoretical physical-layer security does not need to make any assumption of the computational power of the attacker, and, in addition, the security of a communication link can be exactly measured.

Physical-layer security work was pioneered by Shannon and evolved by Wyner in [1], where a discrete memoryless wiretap channel was examined for secure communications in the presence of an eavesdropper. Perfectly secure data transmission can be achieved if the channel capacity of the legitimate link is higher than the eavesdropper link (from source to eavesdropper). In [2], Wyners results were extended to Gaussian wiretap channel: a new metric, the secrecy capacity, was proposed. The secrecy capacity was derived as the difference between the channel capacity of the legitimate link and of the eavesdropper link. If the secrecy capacity is above zero, the legitimate source can adapt the data rate in order to let the destination decode the information, while the data overheard by the eavesdropper is too few and noisy to be decoded. If the secrecy capacity falls below zero, the transmission from source to destination becomes completely insecure, and the eavesdropper can succeed in interpreting the data. In order to improve the security against eavesdropping attacks, one solution is to reduce the probability of occurrence of an intercept event through enlarging the secrecy capacity.

As a consequence, there are extensive works aimed at increasing the secrecy capacity of wireless communications by exploiting multiple antennas [3] and/or cooperative relays [4].

A. Related Works

There are some examples in literature of papers attempting to create a physical region to face the randomness of the

eavesdropper location and/or the amplitude fluctuation due to fading. All these attempts are basically based on the use of multiple antennas and beamforming [5], [10]–[12]. These works aim at building a region as small as possible where the message can be considered secure. The region is built by using beamforming and/or antenna coding between the legitimate transmitter and receiver, or with the help of friendly surrounding nodes (artificial noise injection, jamming). Actually, the definition of the physical region can differ from paper to paper, but mainly beamforming or jamming are used in the works based on information-theoretical parameters, in the form of antenna arrays [10] or distributed antennas [5].

In [6] secrecy rate maximization and power consumption minimization for a multiple-input multiple-output (MIMO) secrecy channel is investigated. A multiantenna cooperative jammer is employed to improve secret communication in the presence of a multiantenna eavesdropper. In [7] and [8] a phase-shifting array is used to produce security in a given direction (directional modulation). The resulting signal is direction-dependent and thus the signal can be purposely distorted in other directions but the desired one. This approach can be used to enhance the security of multiuser multiple-input multiple output (MIMO) communication systems when a multiantenna eavesdropper is present [9].

The metric used to measure the security of the legitimate link is always the received signal to noise plus interference ratio (SINR) or the secrecy outage. The metric, such as the secrecy outage, is well known in literature and it is related to the quality of the legitimate link, given the position of transmitter and receiver, the transmit parameters (power, coding, beamforming, etc.), as well as the location of eavesdropping nodes and interference sources. Other papers based on information-theoretical security typically use the metrics such as secrecy capacity or secrecy outage to measure the security level of the legitimate link by supposing to know the positions and the channel state information of the eavesdroppers and interferers. In order to drop out the dependence on the positions of the eavesdropping or interference nodes,¹ a more general secrecy metric which is basically a characteristic of the network topology can be reached by averaging out the secrecy capacity over all the possible positions of eavesdroppers or interferers [13], [14]. Anyway, all the above mentioned papers deal with metrics which express a characteristic of the link, not of the surface where the link is immersed.

B. Our Contribution

The secrecy capacity is a good metric to evaluate how much is secure a single communication link. But in many practical scenarios a metric which is related to the specific environment can be more effective. For this reason we propose and test here a new metric which bonds the secrecy to the surface of the environment. We named this metric *secrecy pressure*, taking an analogy from the weather forecasting. The secrecy pressure is defined as the secrecy capacity insisting over the infinitesimal element of the surface. This metric can

be used for several practical scopes: from deriving the secrecy of a specific surface/environment, to calculate which is the optimum transmitting antenna orientation or friendly jammer position.

Differently from traditional metrics such as the conventional secrecy capacity, our metric does not imply to know where Eve is. To be more clear, in our approach the secrecy capacity is calculated for each point (x, y) of a surface S . To do this we suppose that Eve is located in (x, y) . Then, we integrate over x and y along the surface S , thus eliminating the dependence on the position of the eavesdropper. The integration operation is, de facto, as taking the average over the space (instead of time). The resulting metric is the secrecy capacity than the entire surface S has got. We call this metric secrecy pressure since it tells how much security insists over a surface S . In other words, we calculate how much secure is an environment, given the position of Alice, Bob and (if present) interferers. It is more practical because 1) we do not have to make any assumptions on the position of the eavesdropper; 2) the new metric is a property of the environment, and not of the point where Eve is located; 3) we calculate a number which gives an insight on how much secure is the environment were going to transmit. The closest concept to this new metric is the network secrecy developed by M. Win *et al.* [13]. The network secrecy is a metric which evaluates the secrecy of an entire network of nodes (not an environment). Legitimate nodes and eavesdropping nodes are randomly distributed as Poisson point processes (PPP). The secrecy capacity is calculated for each legitimate link, given the position of the eavesdroppers. The dependence on the eavesdroppers positions is dropped by averaging out respect to all possible realization of the PPP distribution of the eavesdropper nodes.

The paper also includes a general framework which evaluates the secrecy capacity over a surface. The framework describes all the parameters affecting the secrecy capacity: spatial distribution of the nodes (legitimate and interfering) on a surface, antennas' orientations and patterns, path loss and fast fading statistics of the communication links, transmitting powers. No hypothesis is made over the position of the eavesdroppers, the metric is calculated over the entire surface, as the eavesdropper could be in each point of the surface. Static as well as statistical mobility model are supposed for the eavesdropper. The results show how the metric can be useful in giving an immediate insight on the leakage zones in the surface, and how to adjust the parameters in order to maximize the secrecy. The optimization problem is here formulated for the transmitting antenna orientation and for the position of a friendly jammer.

It is important to highlight that the secrecy pressure does not need to know the position of the eavesdropper (Eve) on the surface of interest. Typically the papers in literature assume to know the position of Eve, which is usually an unpractical assumption. The secrecy pressure or the secrecy map parameters are calculated by assuming that Eve can stay in each point of the surface. If no information about eavesdropper is known, it could be located in any point of the surface with equal probability. We did not introduce a PPP distribution of eavesdropping nodes, although this is a

¹The eavesdroppers and interferers are supposed to be spatially distributed around the legitimate link with a point poisson process (PPP) distribution.

186 common approach, since we suppose that Eve can stay in each
 187 point of the surface. Typically, the PPP distribution is used
 188 to calculate how many eavesdroppers are within the range of
 189 the legitimate transmitter, and then average out the secrecy
 190 capacity. Our approach is different, we are interested in a
 191 new metric which is a characteristic of the surface. Anyway,
 192 a PPP distribution for the presence of Eve over the surface
 193 can be easily assumed in our case too. The secrecy pressure
 194 contains all the parameters that can cause a variation of the
 195 secrecy capacity, and thus it can be optimized respect to many
 196 (known) parameters (transmit antenna orientation, interference
 197 node positions or powers, etc.), separately or jointly.

198 Another known metric in information-theoretical physical-
 199 layer security is the secrecy outage, i.e., the probability that
 200 the secrecy capacity is below a target rate. We have derived
 201 here the secrecy outage probability of a surface (SOPS). In this
 202 case we have supposed that the presence of Eve on the surface
 203 is not perfectly known, but it has an uncertain which we have
 204 modelled as a Gaussian distribution.

205 The instant fading coefficient of Eve's channel should be
 206 anyway known or estimated in order to derive the secrecy
 207 pressure instant by instant. This estimation can be relaxed
 208 if the evaluation of the secrecy pressure is done in ergodic
 209 channel. The ergodic secrecy pressure can be a useful tool in
 210 many practical applications.

211 Practical applications of the propose metric could be tactical
 212 communications: a scenario in which the transmission cannot
 213 surely be overheard in a particular zone of the surface. Another
 214 scenario could be when the information cannot be leaked along
 215 a specific path or street, where the eavesdropper is supposed
 216 to move.

217 The remainder of this article is organized as follows. Sec. II
 218 describes the system model; the framework for the evaluation
 219 of the secrecy capacity over a surface is introduced, including
 220 all the parameters on which it depends, antenna orientation and
 221 pattern, nodes position and power, etc. In Sec. III, the new
 222 metric called secrecy pressure is defined. Sec. IV proposes
 223 the optimization problems, analytical solutions and graphs.
 224 In Sec. V some practical application scenarios are considered;
 225 antenna orientation as well as friendly jammer problems are
 226 solved in specific scenarios: from forbidden zone to mobility
 227 of the eavesdropper. In Sec. VI the closed-form of the secrecy
 228 outage probability of a surface is derived and discussed.
 229 Sec. VII concludes the paper.

230 II. SYSTEM MODEL

231 Consider a 2D surface S described by Cartesian coordinates
 232 (x, y) . Into this space there are the legitimate transmitter
 233 (node i) and receiver (node j), as well as a given number
 234 of interferers I_k with $k = 1, \dots, N_I$ (Fig. 1). For better
 235 comprehension, let's assume that the space is a geographical
 236 urban area, the transmitter is a base station, the receiver
 237 is a mobile terminal and the interferers are other base
 238 stations or access points. We do not assume any specific
 239 position for the eavesdropper in the space. In fact, we want
 240 to derive how the secrecy is mapped all over the given
 241 environment.

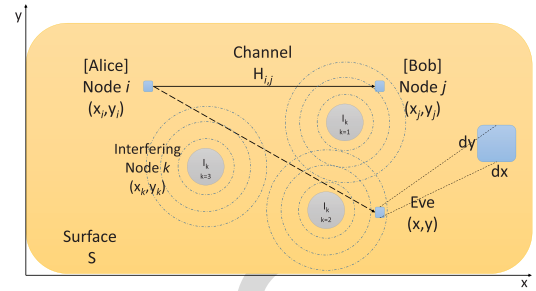


Fig. 1. General scenario. Two legitimate nodes (i and j) want to exchange a confidential message. They are immersed in an environment S together with interfering nodes I_k . The eavesdropper node can be located anywhere over the surface.

242 A. The Scenario

243 We assume to have a surface S where Alice and Bob are
 244 located and their position is known (Fig. 3). In the environ-
 245 ment S there are also interfering nodes, whose positions are
 246 also known. Interfering nodes could be intentional jamming
 247 sources or simply other systems (base stations) radiating in
 248 the same frequency band of the legitimate transmission. To
 249 simulate this scenario, the position of Alice and Bob was
 250 chosen deterministically, while the position of the interfering
 251 nodes were randomly selected, by using a Point Poisson
 252 Process (PPP) distribution. The use of a PPP distribution for
 253 interfering nodes dispersion around a receiver is common in
 254 the literature, when dealing with security of wireless commu-
 255 nications. Alice wants to transmit a confidential message M
 256 to Bob. The legitimate receiver (Bob) tries to recover the message
 257 from the observation vector Z_B . The eavesdropper (Eve) can
 258 be located anywhere in the surface S , and tries to recover
 259 the message M by analyzing the observation vector Z_E . The
 260 wireless channels from Alice to Bob and to Eve are supposed
 261 to be statistically independent.

262 B. Channel Model

263 Let us suppose to have two nodes on the surface S ,
 264 a transmitting node i with position (x_i, y_i) and a receiving
 265 node j with position (x_j, y_j) . The channel between node i
 266 and node j is modeled as

$$267 H_{i,j} = h_{i,j}(\tau, \psi) \cdot d_{i,j}^{-b} \quad (1)$$

268 where $d_{i,j}$ is the Euclidian distance between the nodes, b is
 269 the path loss exponent and $h_{i,j}(\tau, \psi)$ models the multipath
 270 fading effect, including angular dispersion

$$271 h_{i,j}(\tau, \psi) = \sum_{l=1}^L h_{i,j}^{(l)} \delta(\tau - \tau_l) \delta(\psi - \psi_l) \quad (2)$$

272 The parameter τ_l is the delay of arrival of the l -th path, while
 273 ψ_l is the angle of arrival of the l -th path, i.e., τ and ψ
 274 are modeling the time and angular dispersion of the multiple
 275 echoes arriving at the receiver, respectively. The variable
 276 $h_{i,j}^{(l)} = a_{i,j}^{(l)} e^{-\beta_{i,j}^{(l)}}$ denotes the channel coefficient, where $a_{i,j}^{(l)}$
 277 is modelled as a stochastic variable with Rayleigh distribution

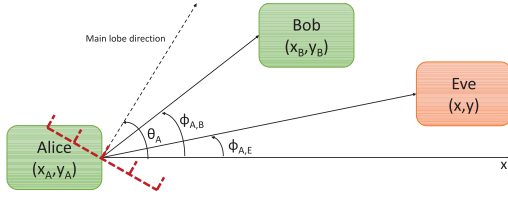


Fig. 2. Antenna pattern of the legitimate transmitter (Alice).

278 whose probability density function (PDF) is

$$279 \quad f_{a_i^{(l)}}(a) = \frac{2a}{\sigma_a} e^{-\frac{a^2}{\sigma_a^2}}$$

280 with σ_a representing the standard deviation of the Rayleigh
 281 distribution, and $\beta_{i,j}^{(l)}$ is modeled as a stochastic random
 282 variable with uniform distribution in $(0, 2\pi)$. Each link that
 283 connect two nodes on the surface is supposed to have a fading
 284 coefficient which is independent to all others.

285 C. Received Power

286 Let us suppose that the node i is transmitting with power P_i .
 287 The power received by the node j is

$$288 \quad P_j = P_i |H_{i,j}|^2 G_i(\theta_i, \phi_{i,j}) G_j(\theta_j, \phi_{j,i}) \quad (3)$$

289 where $G_i(\theta_i, \phi_{i,j})$ is the antenna pattern gain of the
 290 transmitter, $\phi_{i,j}$ is the angle between the x -axis and the
 291 segment connecting node i and j , and θ_i is the angle between
 292 the x -axis and the direction of maximum radiation (main
 293 lobe) of i -node's antenna. Fig. 2 shows the angles mentioned
 294 above, when node i is the legitimate transmitter, called Alice,
 295 and node j is the legitimate receiver, called Bob.

296 Defining $\tilde{P}_{i,j} = P_i G_i(\theta_i, \phi_{i,j}) G_j(\theta_j, \phi_{j,i})$ we can
 297 rewrite (3) as

$$298 \quad P_j = \tilde{P}_{i,j} |H_{i,j}|^2 \quad (4)$$

299 Given the position of node i and j on the surface S , the
 300 angles $\phi_{i,j}$ and $\phi_{j,i}$ are fixed. Then, $\tilde{P}_{i,j} = \tilde{P}_{i,j}(\theta_i, \theta_j)$.
 301 If, in addition, the receiving node j has isotropic antenna
 302 $\theta_j = \text{Const} \forall j$, then $\tilde{P}_{i,j} = \tilde{P}_{i,j}(\theta_i)$.

303 According to [18] and [19], the time dispersion of the
 304 multipath at the receiver has an exponential distribution

$$305 \quad f_\tau(\tau) = \frac{1}{\sigma_\tau} e^{-(\tau-\tau_0)/\sigma_\tau}$$

306 while the angle dispersion of the multipath at the receiver has
 307 a Laplacian distribution

$$308 \quad f_\psi(\psi) = \frac{1}{\sqrt{2\sigma_\psi^2}} e^{-\sqrt{2}(\psi-\psi_0)/\sigma_\psi}$$

309 In order to average out the time and angular dispersion,
 310 the power P_j has to be integrated over all possible times and
 311 angles of arrival

$$312 \quad \bar{P}_j = \tilde{P}_{i,j} d_{i,j}^{-2b} \int_{\tau} \int_{\psi} |h_{i,j}(\tau, \psi)|^2 f_\tau(\tau) f_\psi(\psi) d\tau d\psi \quad (5)$$

D. Aggregate Interference

313 Let us suppose that the N_I interfering nodes are distributed
 314 on the surface S following a point Poisson process (PPP)
 315 distribution with density λ . The sum of the interference power
 316 at the node j is
 317

$$318 \quad \mathbf{I}_j = \sum_{k=1}^{N_I} P_k G_k(\theta_k, \phi_{k,j}) G_j(\theta_j, \phi_{j,k}) d_{k,j}^{-2b} |h_{k,j}|^2$$

$$319 \quad = \sum_k \tilde{P}_{k,j} |H_{k,j}|^2 \quad (6)$$

320 where P_k is the power emitted by the k -th interfering node,
 321 $d_{k,j}$ is the Euclidian distance between the k -th interfering
 322 node and node j and $h_{k,j}$ is the channel coefficient associated
 323 to the link (1). If the position of the N_I interfering nodes
 324 (x_k, y_k) with $k = 1, \dots, N_I$ is fixed, then $\tilde{P}_{k,j} = \tilde{P}_{k,j}(\theta_k, \theta_j)$.
 325 If, in addition, the receiving node j has isotropic antenna
 326 $\theta_j = \text{Const} \forall j$, then $\tilde{P}_{k,j} = \tilde{P}_{k,j}(\theta_k)$. In this case, the
 327 aggregate interference \mathbf{I}_j is a random variable with Stable
 328 distribution [16], [17]

$$329 \quad \mathbf{I}_j \sim S(\alpha, 1, \gamma_j) \quad (7)$$

330 where $\alpha = 1/b$ and

$$331 \quad \gamma_j = \pi \lambda \Xi_\alpha^{-1} \mathbb{E} \left\{ \left(\sum_k \tilde{P}_{k,j} |h_{k,j}|^2 \right)^\alpha \right\}$$

332 with

$$333 \quad \Xi_\alpha = \begin{cases} \frac{1-\alpha}{\Gamma(2-\alpha) \cos(\pi\alpha/2)} & \text{if } \alpha \neq 1 \\ \frac{2}{\pi} & \text{if } \alpha = 1 \end{cases} \quad (8)$$

334 where $\Gamma()$ denotes the Gamma distribution function and $\mathbb{E}\{\}$
 335 the expectation operator.

336 The PDF of \mathbf{I}_j is

$$337 \quad f_{\mathbf{I}_j}(I) = \frac{1}{2\pi} \int \varphi_I(\omega) e^{-j\omega I} d\omega$$

$$338 \quad = \frac{1}{\pi} \int_0^\infty e^{-\omega^\alpha \gamma_j} \cos \left[\tan \left(\frac{\pi\alpha}{2} \right) \omega^\alpha \gamma_j - \omega I \right] d\omega \quad (9)$$

339 where

$$340 \quad \varphi_I(\omega) = \exp \left\{ -|\omega|^\alpha \left[1 - j \text{Sgn}(\omega) \tan \left(\frac{\pi\alpha}{2} \right) \right] \gamma_j \right\}$$

341 is the characteristic function of the random variable I .

342 It is important to highlight that depending on the position
 343 of the receiver j on the surface S , not all the N_I interferers
 344 could affect the receiver. The distance (path loss) $d_{k,j}^{-2b}$
 345 could be close to zero, thus the node k does not contribute to the
 346 aggregate interference at the receiver j .
 347

III. SECRECY PRESSURE AND SECRECY FORCE

348 We want to define a new metric that allows to measure
 349 the intensity of secrecy over a given surface. Taking analogy
 350 from the atmospheric weather science, we define the concept
 351 of *Secrecy Pressure*.
 352

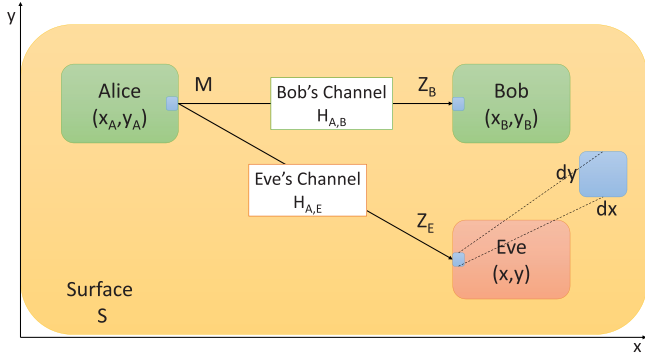


Fig. 3. Scheme of the transmission of the confidential message M from Alice to Bob.

Let us now associate the previous defined transmitting node i as Alice and the receiving node j as Bob. Alice is then located at point (x_A, y_A) and Bob at (x_B, y_B) on the surface S . The position of the eavesdropper Eve is not known, thus we suppose that its coordinates are generically (x, y) .

Suppose that Alice wants to transmit a confidential message M to Bob. Bob tries to recover the information M from the vector Z_B received (Fig. 3). Given the model in Sec. II, the mutual information exchanged in the legitimate link (from Alice to Bob) is

$$\mathbb{I}_B = \mathbb{I}(M; Z_B) = \mathbb{H}(M) - \mathbb{H}(M|Z_B) \quad (10)$$

where $\mathbb{H}()$ denotes the entropy.

Analogously, the eavesdropper (Eve) tries to recover the message M from the received vector Z_E . Thus, the information stolen by Eve is

$$\mathbb{I}_E = \mathbb{I}(M; Z_E) = \mathbb{H}(M) - \mathbb{H}(M|Z_E) \quad (11)$$

The term $\mathbb{I}(M; Z_E)$ is called Leakage, and it denotes the amount of information on the message M that Eve is able to recover from the received vector Z_E .

As known, these two mutual information can be used to calculate the secrecy capacity [15]

$$C_{sec} = \max_{\mathfrak{p}_M} \{\mathbb{I}_B - \mathbb{I}_E\} \geq \max_{\mathfrak{p}_M} \mathbb{I}_B - \max_{\mathfrak{p}_M} \mathbb{I}_E = C_B - C_E \quad (12)$$

where C_B and C_E are the capacities of Bob's and Eve's channel, respectively, and \mathfrak{p}_M is the marginal distribution of the codeword M . The secrecy capacity is at least as large as the difference between the legitimate channel capacity and the eavesdroppers channel capacity. The inequality can be strict as in the case of complex Gaussian wiretap channels [15], as well as typical wireless fading channels, which are here considered. It is important to note that both \mathbb{I}_B and \mathbb{I}_E depend on the channel state and position of Bob and Eve respect to Alice, respectively. This means that changing the position of Bob or Eve on the surface S , the mutual information changes.

The capacity of the link between the transmitter, called Alice, positioned in (x_A, y_A) , and the position (x_B, y_B) of the legitimate receiver, called Bob, can be written as

$$C_B = \frac{1}{2} \log \left(1 + \frac{P_B}{N_0 + \mathbf{I}_B} \right) \quad (13)$$

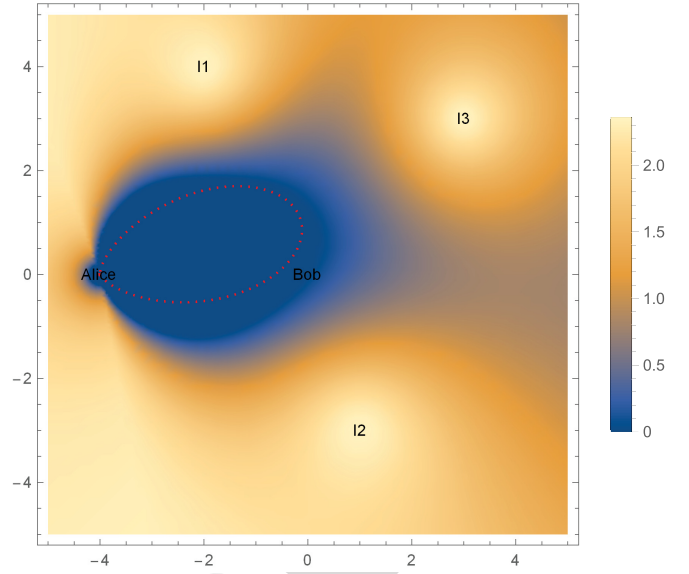


Fig. 4. Secrecy map of surface S with Alice's antenna orientation and pattern. Three interfering nodes (I_1, I_2, I_3) are present. The azimuth of Alice transmission antenna is 6 deg.

where N_0 denotes the Gaussian noise density at the receiver, P_B and \mathbf{I}_B are defined in (4) and (6), respectively.

Since typically we cannot know if an eavesdropper, called Eve, is present in the surface S or where it is located, we derive the capacity of a generic point (x, y) of the surface, i.e.,

$$C_E(x, y) = \frac{1}{2} \log \left(1 + \frac{P_E}{N_0 + \mathbf{I}_E} \right) \quad (14)$$

where P_E and \mathbf{I}_E are defined as in (4) and (6), respectively

$$P_E = P_A G_A(\theta_A, \phi_{A,E}) G_E(\theta_E, \phi_{E,A}) d_{A,E}^{-2b} |h_{A,E}|^2 \quad (15)$$

$$\mathbf{I}_E = \sum_{k=1}^{N_I} P_k G_k(\theta_k, \phi_{k,E}) G_E(\theta_E, \phi_{E,k}) d_{k,E}^{-2b} |h_{k,E}|^2$$

Thus, supposing that Eve is located in a generic point (x, y) on the surface S , the secrecy capacity of the link between Alice and Bob is

$$C_{sec}(x, y) = \max\{0, C_B - C_E(x, y)\} = [C_B - C_E(x, y)]^+ \quad (15)$$

It is important to highlight that the capacities here are intended as conditioned to the state of the channels $h_{A,B}$, $h_{A,E}$, $h_{k,B}$ and $h_{k,E}$, as well as the state of the aggregate interference \mathbf{I}_B and \mathbf{I}_E .

What we are proposing here is to define a secrecy capacity for each elementary point (x, y) of the surface S . Using this representation, we can elaborate a map of the secrecy of the surface given the position of the known actors, i.e., legitimate users and interfering nodes. In other words, given the positions of Alice, Bob and interfering nodes I_k , for each point (x, y) of the surface, we calculate the secrecy capacity of the legitimate link as Eve was located in that point. The result is that we can draw a map showing the different levels of secrecy of the entire surface S (Fig. 4).

418 The *Secrecy Pressure* p_{sec} is defined as

$$419 \quad p_{sec} = \frac{1}{A_S} \iint_S C_{sec}(x, y) dx dy = \frac{F_{sec}}{A_S} \quad (16)$$

420 where A_S denotes the area of the surface S and the term F_{sec}
421 is denoting what we define as *Secrecy Force*. The secrecy force
422 depends on the locations of the legitimate users and interfering
423 nodes, but not on the eavesdroppers. The metric p_{sec} is a useful
424 parameter that indicates how much is secure a surface S , given
425 the position of legitimate nodes and interfering nodes. Using
426 this metric, different surfaces and/or nodes configurations can
427 be thus ordered

$$428 \quad p_{sec}^{(1)} < p_{sec}^{(2)} < p_{sec}^{(3)} < \dots$$

429 The index allows a ranking of a given spatial configuration of
430 legitimate entities and interferes.

431 Detailing Eq. (16), we can find an interesting property of
432 the secrecy pressure

$$433 \quad p_{sec} = \frac{1}{A_S} \int_x \int_y \begin{cases} 0 & \text{if } C_B \leq C_E(x, y) \\ C_B - C_E(x, y) & \text{if } C_B > C_E(x, y) \end{cases} dx dy \quad (17)$$

435 Since C_B does not depend on (x, y) , if the surface goes to
436 infinity, the secrecy pressure tends to a constant value

$$437 \quad \lim_{S \rightarrow \infty} p_{sec} = \lim_{S \rightarrow \infty} \left(\frac{1}{A_S} \iint_S [C_B - C_E(x, y)]^+ dx dy \right) = C_B \quad (18)$$

439 This is because the path loss component $d_{A,E}^{-2b}(x, y)$ in (3)
440 vanishes as the generic point (x, y) on the surface S goes
441 to infinity. In practice, the contributions that decrease the
442 secrecy pressure mainly comes from the points on the surface
443 close to the legitimate link. In other words, supposing to
444 have an infinite surface, the set of points where Eve could be
445 located that influence the secrecy capacity is limited, due to
446 the path-loss. A point (x, y) too far away from the legitimate
447 nodes cannot affect the secrecy capacity, since the legitimate
448 signal is received with a too low power to observe anything
449 ($C_E(x, y) = 0$).

450 From Eq. (15) we can derive another useful representation,
451 called *Secrecy Map*. The $C_{sec}(x, y)$ in (15) is indicating
452 which is the secrecy capacity insisting over the elementary
453 unit surface $dx dy$ located in a generic point (x, y) of
454 the surface S (see Fig. 3). This representation can be used to
455 draw the behaviour of the secrecy capacity over the surface S ,
456 showing zones where the secrecy is low or high, analogously
457 to the weather forecast (Fig. 4). The map, in fact, is built by
458 calculating the secrecy capacity of the legitimate link as the
459 eavesdropper was located in each point of the surface. The blue
460 zones in Fig. 4 indicate no secrecy, i.e., if the eavesdropper
461 is set there, the secrecy rate of the legitimate link is zero.
462 Summarizing, the secrecy map is derived by the following
463 steps:

- 464 1) take a surface with cartesian coordinates;
- 465 2) locate the legitimate nodes (Alice and Bob) on the
466 surface;

- 467 3) compute the secrecy capacity of the legitimate link
468 assuming that Eve is located in a point (x, y) of the
469 surface;
- 470 4) associate that secrecy capacity to the corresponding
471 point of the surface;
- 472 5) repeat 3 and 4 for every point of the surface.

473 The secrecy capacity associated to a generic point of the
474 surface could be zero, i.e., any time Eve has a greater channel
475 capacity compared to Bob.

476 The secrecy map of the surface S changes with

- 477 • the positions of Alice, Bob and interfering nodes I_k
478 ($k = 1, \dots, N_I$);
- 479 • the pattern and the orientation $G_A(\theta_A)$ of the legitimate
480 transmitter antenna;
- 481 • the power of the legitimate transmitter P_A ;
- 482 • the power of the transmitters of the interfering nodes P_k ;
- 483 • the state $h_{A,B}$, $h_{A,E}$, $h_{k,B}$ and $h_{k,E}$ of the channels.

484 The effect of time and angle dispersion at the receivers can
485 be averaged out by replacing \bar{P}_j with $j = B$ in (13) and with
486 $j = E$ in (14).

487 As listed in the above items, the secrecy capacity in (15)
488 depends on the instant fading coefficients $h_{A,B}$, $h_{A,E}$, $h_{k,B}$
489 and $h_{k,E}$. This means that the secrecy pressure (16) (and the
490 secrecy map) depends instantly on these processes. In order
491 to remove the dependance on the instantaneous realizations
492 of the fading coefficients, two solutions can be run: 1) put
493 the characteristic function of the fading coefficients into the
494 secrecy capacity formula and average it out, or more easily,
495 2) assume that the channels are ergodic. The results shown
496 in this paper are calculated by supposing ergodic channels.
497 Ergodic-fading model characterizes a situation in which the
498 duration of a coherence interval is on the order of the time
499 required to send a single symbol. The processes $h_{A,B}$, $h_{A,E}$,
500 $h_{k,B}$ and $h_{k,E}$ are mutually independent and i.i.d.; fading coef-
501 ficients change at every channel use and a symbol experiences
502 many fading realizations.

503 The ergodic secrecy capacity is thus [15]

$$504 \quad \tilde{C}_{sec}(x, y) = \mathbb{E}_{|h_{A,B}|^2, |h_{A,E}|^2, |h_{k,B}|^2, |h_{k,E}|^2} \{ [C_B - C_E(x, y)]^+ \} \quad (19)$$

505 $k = 1, \dots, N_I$

506 where the operator $\mathbb{E}\{\}$ stands for the expectation. The ergodic
507 secrecy pressure is obtained by substituting the ergodic secrecy
508 capacity in (19) into Eq. (16)

$$509 \quad \tilde{p}_{sec} = \frac{1}{A_S} \iint_S \tilde{C}_{sec}(x, y) dx dy \quad (20)$$

510 Since $\tilde{C}_{sec}(x, y)$ could be zero in some points of the surface,
511 computing \tilde{p}_{sec} implies to make an integral of an irregular
512 function.

513 It is important to point out that the power received by
514 Eve depends on the position of Eve, since path-loss, fading,
515 angle-of-departure, angle-of-arrival, as well as the power of
516 the aggregate interference are position-dependent parameters.
517 Therefore, in the expression of the capacity of both Bob
518 and Eve, the parameters are position-dependent. Since we
519 want a metric which is not dependent on the position of Eve
520 (its position is not known with 100% probability, typically),

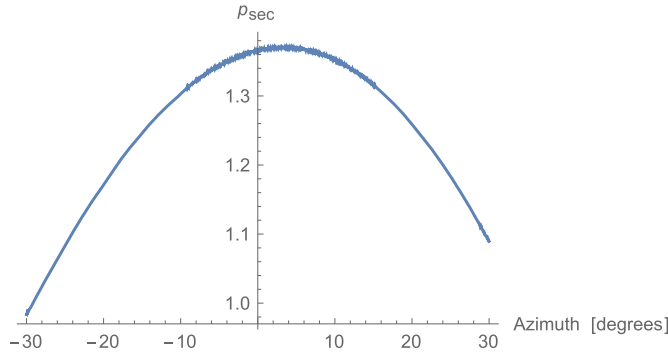


Fig. 5. Secrecy pressure when the optimization problem is solved respect to Alice's antenna orientation.

521 we first locate Eve in each point (x,y) of the surface S , we
 522 calculate the secrecy capacity of each point (x,y) and then we
 523 integrate over the entire surface S . In this way, we take the
 524 mean over a space of the secrecy capacity, which eliminates
 525 the dependence of the secrecy capacity by specific position
 526 of Eve. The resulting (new) metric is a characteristic of the
 527 surface and not of the link, thus we called it secrecy pressure.

IV. SECRECY OPTIMIZATION

528
 529 The secrecy pressure can be used as a useful metric to deter-
 530 mine which is the best configuration parameters to optimize
 531 the secrecy of a link. The proposed metric is suitable to find
 532 out different useful results, such as: a) which is the antenna
 533 orientation that assures highest secrecy towards the legitimate
 534 receiver; b) where is the best location where to put additional
 535 interfering node(s) in order to reach higher secrecy for the
 536 legitimate link; c) which is the best configuration of power
 537 emissions from the interfering nodes in order to have highest
 538 secrecy for the legitimate link.

A. Antenna Orientation

539
 540 Let us suppose for simplicity that the interfering nodes I_k
 541 as well as Bob and Eve have isotropic antennas. Fixed the
 542 surface S , the positions of the legitimate nodes (Alice, Bob)
 543 and of the interfering nodes I_k ($k = 1, \dots, N_I$), and given the
 544 pattern of the transmitting antenna $G_A(\theta_A)$, we can maximize
 545 the secrecy pressure respect to the antenna orientation

$$\arg \max_{\theta_A} \{p_{sec}\} \quad (21)$$

547 Fig. 5 shows the secrecy map over the surface S when
 548 Eve is supposed to be set somewhere in the surface S and
 549 the optimization problem is solved respect to Alice's antenna
 550 orientation. There exists an optimum azimuth orientation of
 551 Alice's antenna. Given the positions of the legitimate users
 552 and interfering nodes, the best, from the secrecy capacity point
 553 of view, for Alice is not to point the maximum of the antenna
 554 pattern towards the direction of Bob. An azimuth orientation of
 555 $+6$ deg optimizes the secrecy capacity, in this case. In general,
 556 with the proposed metric it is possible to derive easily which is
 557 the best antenna orientation for the transmission to a legitimate
 558 receiver in a given perimeter, of which we know only the

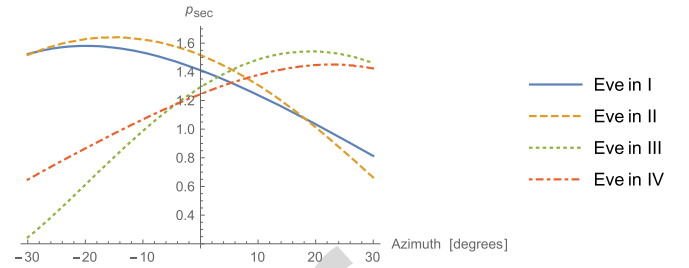


Fig. 6. Secrecy map for different positions of Eve (I, II, III and IV quadrant) when the optimization problem is solved respect to Alice's antenna orientation.

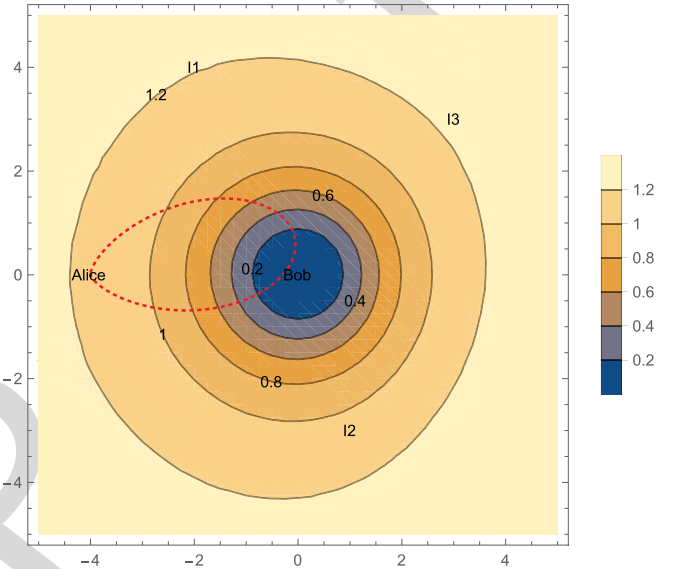


Fig. 7. Secrecy map over the surface S when the optimization problem is solved respect to the position of the additional interfering node (flasher).

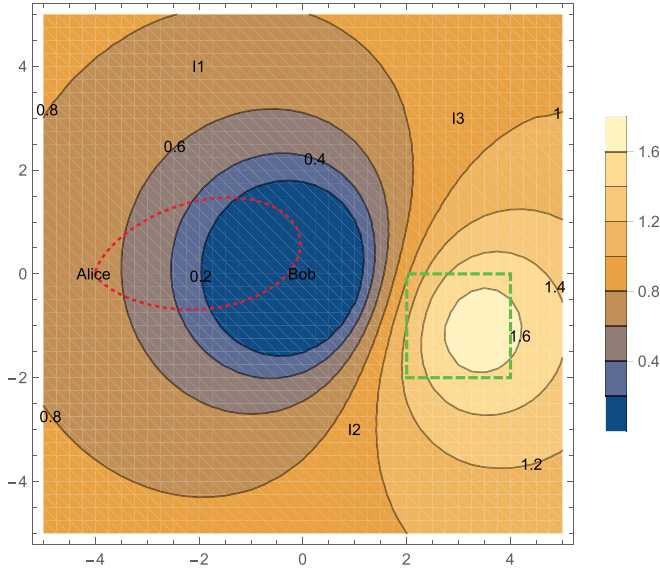
559 positions of the interferers (e.g., other access points or base
 560 stations). Fig. 6 shows the secrecy map over the surface S
 561 for different positions of Eve (I, II, III and IV quadrant)
 562 when the optimization problem is solved respect to Alice's antenna
 563 orientation. As an example, suppose that the legitimate users
 564 do want to minimize the information leakage in a specific
 565 zone of the surface (e.g., the eavesdropper is suspected to be
 566 in the third quadrant), then the optimum antenna orientation
 567 for Alice is $+16$ deg (green curve in Fig. 6).

B. Interfering Node Positions

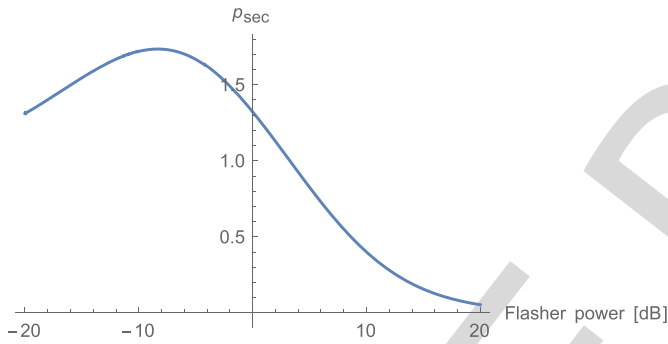
568
 569 Fixed the surface S , the positions of the legitimate nodes
 570 (Alice, Bob) and given the pattern and orientation of the
 571 transmitting antenna $G_A(\theta_A)$, we can maximize the secrecy
 572 pressure over the position (x_k, y_k) of the $N_I + 1$ -th interfering
 573 node, a friendly jammer called here *flasher*, in order to
 574 maximize the secrecy pressure of the legitimate link, given
 575 the positions (fixed) of the N_I interfering nodes

$$\arg \max_{(x_k, y_k), k=N_I+1} \{p_{sec}\} \quad (22)$$

577 Fig. 7 shows the secrecy map over the surface S when the
 578 optimization problem (22) is solved. As it can be seen, there
 579 are positions where the additional interference node (flasher)



(a) Secrecy map over the surface S when the optimization problem is solved respect to the position of the additional interfering node (flasher). Eve is supposed to be somewhere in the green dotted line.



(b) Secrecy pressure as a function of the power of the additional interfering node (flasher). The flasher is supposed to be placed in the center of the lighter zone depicted in Fig. 8(a).

Fig. 8. Optimization of both position and power of the additional interfering node (flasher).

580 can be put which optimize the secrecy pressure metric. Like
 581 forecast weather, the areas with same color bring the same
 582 secrecy capacity, if the additional interfering node (friendly
 583 jammer) is installed in that point of the surface. Another
 584 evident result is that the interfering node cannot be placed
 585 close to Bob (white hole in Fig. 7), since the this would
 586 decrease drastically the capacity of the legitimate link and thus
 587 the secrecy capacity. Fig. 8(a) shows the same secrecy map in
 588 the case that Eve is supposed to be somewhere in a limited
 589 perimeter (the green dotted line) inside the surface S . In this
 590 case the optimum area is modified compared to the previous
 591 scenario.

592 C. Power Allocation of the Interferers

593 Fixed the surface S , the positions of the legitimate nodes
 594 (Alice, Bob) and of the interfering nodes² I_k , and given the
 595 pattern and orientation of the transmitting antenna $G_A(\theta_A)$,

²The position of the interfering nodes has been randomly selected by using a PPP distribution.

we can maximize the secrecy pressure respect to the power
 emitted by the interfering nodes

$$\arg \max_{P_k} \{p_{sec}\} \quad k = 1, \dots, N_I \quad (23)$$

To ease the illustration of this optimization, let us suppose
 to put an additional interfering node (the 4th) in the scenario
 and to optimize its transmit power. Figs. 8(a) shows the secrecy
 map over the surface S when the optimization problem is
 solved respect to the position of the additional interfering node
 (flasher) and its power. The eavesdropper is supposed to be
 located somewhere in a limited perimeter (the green dotted line
 in the figure) of the surface. The lighter zone of the secrecy
 map denotes the set of points (x,y) where the flasher can be
 located to yield the highest secrecy pressure. Fig. 8(b) shows
 the secrecy pressure as a function of the power of the flasher.
 The curve evidently shows an optimum point, which in that
 case is about -9 dB.

It is important to stress that using the proposed metric the
 optimum antenna orientation is not trivially in the direction of
 the legitimate receiver, as well as the optimum position and
 power of the intentional jammer (flasher) are not those that
 the common sense would suggest.

D. Joint Optimization

Joint optimization of all the parameters (antenna orientation,
 friendly jammer position and interfering power allocation) is
 also possible

$$\arg \max_{(\theta; (x_k, y_k); P_k)} \{p_{sec}\} \quad k = 1, \dots, N_I \quad (24)$$

Graphical results of this optimization are not shown in this
 paper due to the lack of space.

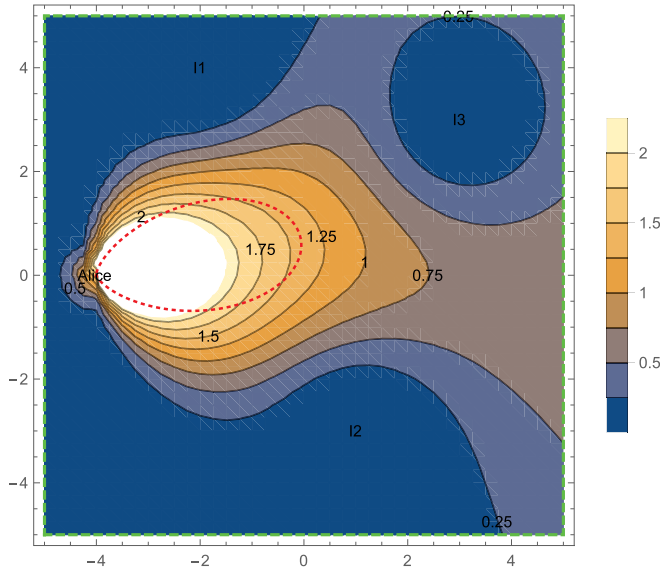
E. Varying the Position of Bob

Although the most practical scenario is when Alice and Bob
 are fixed and Eve can be everywhere in a limited space, as
 previously described, one could also be interested in using the
 proposed metric to draw the map of the secrecy pressure when
 Bob's position can vary over the surface S . In this case, the
 steps to draw the map are the following

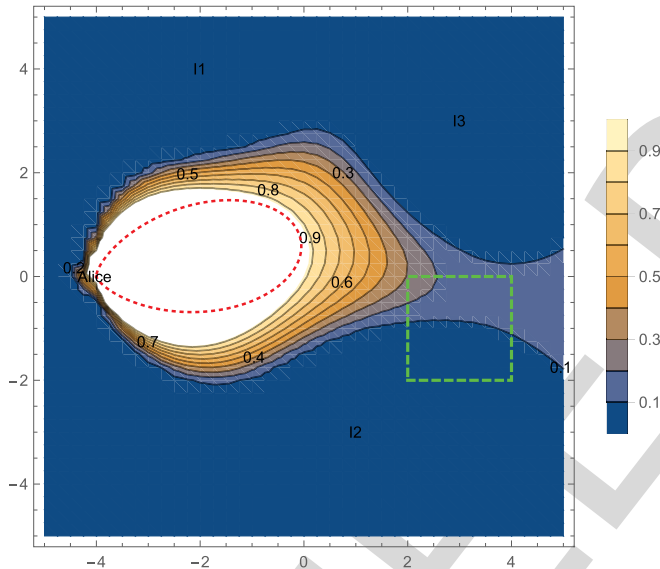
- locate the legitimate receiver (Bob) in a point (x, y) of the surface S ;
- calculate the secrecy pressure metric (20) for Bob located in that point;
- assign to the point (x, y) the value of the secrecy pressure;
- repeat these points until all the surface S is evaluated.

Fig 9(a) shows the map of the secrecy pressure when Bob's
 position varies over the surface and Eve's position varies over
 the entire surface as well. As expected the secrecy pressure is
 higher when Bob is inside the main lobe of Alice, while the
 secrecy pressure decreases drastically when Bob is closer to
 an interferer.

Fig 9(b) shows the map of the secrecy pressure when Bob's
 position vary over the surface and Eve's position varies only
 in a limited perimeter (the green dashed line). Compared to
 Fig 9(a), if Eve is confined into a limited space in



(a) Map of the secrecy pressure as a function of Bob's position. Eve can be everywhere over the surface.



(b) Map of the secrecy pressure as a function of Bob's position. Eve is supposed to be somewhere in the green dotted line.

Fig. 9. Map of the secrecy pressure. The secrecy pressure is calculated as Bob was in each point (x, y) of the surface S .

648 the surface S , the zone of maximum secrecy pressure is larger
649 and located around the main lobe of Alice. Please note that the
650 secrecy pressure behind Alice, e.g. the point $(-4, -2)$, is low
651 since there is almost no power from Alice in that direction.

652 V. GENERAL DEFINITION OF SECRECY PRESSURE 653 AND PRACTICAL APPLICATIONS

654 As stated in the previous sections, the new metric is defined
655 starting from the definition of the well-known secrecy capacity
656 (C_{sec}). To eliminate the dependence on the position of the
657 eavesdropper of the secrecy capacity, we have averaged out
658 the secrecy capacity by integrating the C_{sec} over the 2D-space
659 of the specific surface S . The resulting metric is called secrecy

660 pressure and it is the analytical expression of the average over
661 a space (instead of time). The integral of the C_{sec} function is
662 not easy to derive, since C_{sec} shows sparsely zeros over the
663 2D surface, each time that the capacity of Eve is greater of
664 the capacity of Bob. A closed-form expression of the secrecy
665 pressure is not easy to obtain, even for simple geometry shape
666 like circle or square with generic boundaries. For this reason,
667 we have derived the closed-form expression of the secrecy
668 outage of a surface (see Sec. VI). Although a closed-form
669 expression of the secrecy pressure for a known shape is not
670 shown in the paper, this does not mean that the metric makes
671 no sense. The metric is defined as the spatial average of the
672 secrecy capacity calculated for every point of the surface S .
673 The average of the secrecy capacity over time is called ergodic
674 secrecy capacity in the literature, but no previous paper, in our
675 knowledge, presented the spatial average.

676 This metric shows the secrecy as a characteristic of a
677 surface and not of a single link. This is useful in many
678 practical scenarios, like military tactical scenarios. Typically,
679 military command has a specific perimeter of operation, where
680 the presence of the enemy is not perfectly known, based
681 on the information that the intelligence service or technologies
682 (satellite, etc.) can collect. Most probably, the military
683 command can delimit the presence of the enemy in some
684 zones of the operational scenario, associating the presence
685 of the enemy with a certain probability. By calculating the
686 secrecy pressure, the military command can: 1) quantify how
687 much secure is one perimeter from the point of view of the
688 wireless transmissions; 2) decide the optimum angle for the
689 transmitting antenna array; 3) decide which is the optimum
690 position to place a jammer to enhance the security of the
691 transmission; 4) decide the optimum power of the jammer,
692 in order not to degrade the reception of the legitimate receiver
693 while jamming the potential eavesdropper; 5) operate a multi-
694 parameter optimization; 6) if the position of the eavesdropper
695 is only partially known, the military command can draw
696 zones in the operational perimeter giving to each of them a
697 statistical probability of Eve presence, and then compute the
698 secrecy of the perimeter; 7) if a mobility model of Eve is
699 known or partially (statistically) known, again all the above
700 mentioned parameters (antenna orientation, friendly jammer
701 position, etc.) can be optimized. Other optimizations can be
702 further imagined.

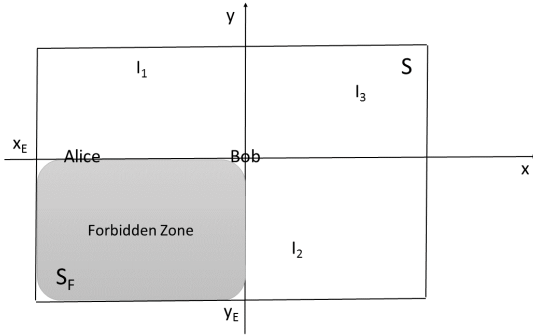
703 As discussed above, in many practical situations we do not
704 know if an eavesdropper is present and where it is located
705 exactly. Thus, we define a probability of presence of Eve to
706 be associated to a generic point (x, y) on the surface S

$$707 \Upsilon_{X,Y}(x, y) = Prob\{x \leq X \leq x + dx, y \leq Y \leq y + dy\} \\ 708 = \int_x^{x+dx} \int_y^{y+dy} v_{X,Y}(x, y) dx dy \quad (25)$$

709 where $v_{X,Y}(x, y)$ is the probability density function (PDF) of
710 the presence of Eve in (x, y) . From now on we call this PDF
711 $v_E(x, y)$.

712 The secrecy pressure is thus re-defined as follows

$$713 p_{sec} = \iint_S v_E(x, y) C_{sec}(x, y) dx dy \quad (26)$$

Fig. 10. Forbidden zone inside the surface S .

714 where $C_{sec}(x, y) = [C_B - C_E(x, y)]^+$ and $\iint v_E(x, y)$
 715 $dx dy = 1$. Eq. (26) represents the more general expression
 716 of the secrecy pressure in (16). For example, if a uniform
 717 distribution of Eve's presence is supposed for the entire
 718 surface S , the PDF would be $v_E(x, y) = 1/A_S$ and thus
 719 $\iint_S 1/A_S dx dy = 1$.

720 In the following sections three practical scenarios are pro-
 721 posed to show the benefits of the new proposed metric.
 722 In particular, the secrecy pressure is computed when

- 723 • an eavesdropper is known to be in a sub-region of the
 724 surface S (leakage zone),
- 725 • the eavesdropper position is known with a probability
 726 spatial function (Gaussian approximation), and
- 727 • when the eavesdropper has not a fixed position (mobility
 728 scenario).

729 In all these cases, some simplifications are assumed

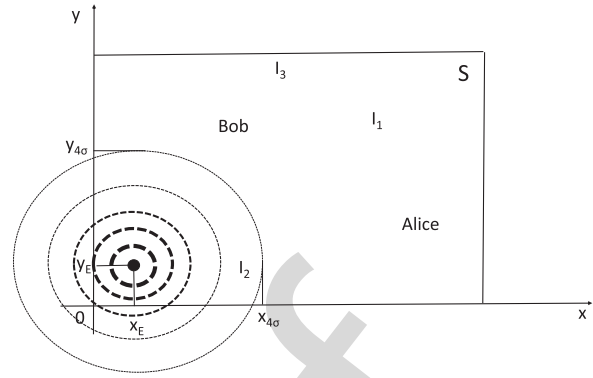
- 730 • the average fading of the channels is supposed to be 1,
 731 i.e., $\sum_l |h_{i,j}^{(l)}|^2 = 1$;
- 732 • the antenna pattern of Bob, Eve and of the interfering
 733 nodes is supposed to be isotropic. Only Alice has a
 734 directive antenna and can modify the antenna orientation;
- 735 • the position of Alice and Bob on the surface S is supposed
 736 to be fixed and known: $(-4, 0)$ and $(0, 0)$, respectively;
- 737 • the position of the interfering nodes (I_1, I_2, I_3) is supposed
 738 to be fixed and known: $(-2, 4)$, $(1, -3)$ and $(3, 3)$,
 739 respectively.

740 A. Leakage Zone

741 In many real situations, e.g., in military scenarios, the
 742 transmitter does not want to leak information in fixed zone,
 743 in a region where it knows that an eavesdropper is surely
 744 present. We name here the leakage zone as *forbidden zone*,
 745 since the legitimate transmitter surely does not want to leak
 746 any information in that zone. Fig. 10 shows the surface S
 747 with the forbidden zone S_F inside. In this example the forbidden
 748 zone is the third quadrant.

749 To each point of the surface S_F we associate a probability
 750 of Eve's presence such that $\iint_{S_F} v_E(S) dx dy = 1$, while in
 751 the rest of the surface S we set $\iint_{-S_F} v_E(S) dx dy = 0$, where
 752 $-S_F$ denotes the complementary surface $S_F \cup -S_F = S$.

753 Assume, as an example, to have an equal distribution
 754 of the probability of Eve's presence in the surface S_F .

Fig. 11. Gaussian distribution of Eve's presence inside the surface S .

755 Than,

$$756 v_E(x, y) = \begin{cases} \frac{1}{x_E y_E}, & \text{if } x \in [0, x_E] \text{ and } y \in [0, y_E] \\ 0, & \text{otherwise} \end{cases} \quad (27)$$

757 In this case the secrecy pressure of the surface (26) is

$$758 p_{sec} = \int_0^{x_E} \int_0^{y_E} v_E(x, y) C_{sec}(x, y) dx dy \quad (28)$$

759 The secrecy map of the surface can be drawn by using the
 760 following result

$$761 v_E(x, y) C_{sec}(x, y) = \begin{cases} 0 & \text{if } C_{sec}(x, y) = 0 \\ C_B - \frac{1}{x_E y_E} \int_0^{x_E} \int_0^{y_E} C_E(x, y) dx dy & \text{otherwise} \end{cases} \quad (29)$$

764 The optimization of the secrecy pressure respect to the
 765 azimuth of the transmitting antenna of the legitimate node
 766 (Alice) for a forbidden zone is shown in Fig. 5.

767 B. Gaussian Probability of Eavesdropper Presence

768 In other situations, it is not known exactly if eavesdroppers
 769 are present or not. Only suspicious. In this case, located a
 770 point on the map, a probability of presence of Eve with
 771 certain distribution can be associated. We suppose here that
 772 a Gaussian spatial distribution of Eve's presence is associated
 773 to a zone of the surface S . To each point of the surface
 774 S we associate a probability of Eve's presence v_E which
 775 is a random variable with Gaussian distribution centered in
 776 (x_E, y_E) (Fig. 11). The circle lines denotes the intensity of
 777 the probability. For example, if the Gaussian random variable
 778 denoting the presence of Eve on the surface has mean 0.8 and
 779 variance 1, we associate a probability of Eve's presence equal
 780 to 0.8 to the point (x_E, y_E) .

781 In this case the secrecy pressure of the surface (26) is

$$782 p_{sec} = \iint_S v_E(x, y) C_{sec}(x, y) dx dy \quad (30)$$

783 With $v_E(x, y) = \frac{1}{\sqrt{2\sigma_E^2}} e^{-\frac{(x-x_E)^2 + (y-y_E)^2}{2\sigma_E^2}}$, where σ_E indicates the
 784 standard deviation of the Gaussian distribution.

785 The secrecy map of the surface can be drawn by using the
786 following result

$$787 \quad v_E(x, y)C_{sec}(x, y)dxdy$$

$$788 \quad = \begin{cases} 0 & \text{if } C_{sec}(x, y) \leq 0 \\ C_B - \iint_S v_E(x, y)C_E(x, y)dxdy & \text{otherwise} \end{cases}$$

789 (31)

790 This scenario is a particular case of the mobility scenario
791 described in the next section, the results can be appreciated
792 in Fig. 13(b).

793 C. Mobility Model for the Eavesdropper

794 If we know the position of Eve at time t_n , we can associate
795 to the eavesdropper a statistical mobility model and derive the
796 secrecy pressure over a surface of interest. The mobility model
797 for Eve depends on its movement capability in the specific
798 environment. In the absence of prior information on the real
799 movement of the eavesdropper (i.e., Eve is free to move in all
800 directions with different speeds), the Gaussian mobility model
801 represents a fairly general model with a tractable number of
802 parameters. In the presence of some prior information on the
803 eavesdroppers movement (e.g., direction or speed is set by the
804 environment), a mobility model more tight to the real mobility
805 would provide better performance.

806 Optimization of the secrecy pressure is shown respect to
807 the azimuth of the legitimate transmitting antenna as well as
808 respect to the position of the flasher.

809 We consider here Gaussian mobility model with conditional
810 PDF of current position conditioned on the previous position.
811 For easier notation, let us define the position (x, y) at time t_n
812 of a point on the surface S as a vector \mathbf{p}_n . Thus, the conditional
813 PDF of current position is

$$814 \quad v_m(\mathbf{p}_n|\mathbf{p}_{n-1}) = \frac{1}{2\pi|\Sigma_m|^{\frac{1}{2}}} e^{-\frac{1}{2}[(\mathbf{p}_n - \boldsymbol{\mu}_n)^T \Sigma_m^{-1}(\mathbf{p}_n - \boldsymbol{\mu}_n)]} \quad (32)$$

815 where $\boldsymbol{\mu}_n$ varies with the mobility model as described in
816 the following, and the covariance matrix Σ_m accounts for
817 the uncertainty in the movements in a 2-D plane; thus, it is
818 expressed by

$$819 \quad \Sigma_m = \begin{bmatrix} \sigma_{m,x} & \rho\sigma_{m,x}\sigma_{m,y} \\ \rho\sigma_{m,x}\sigma_{m,y} & \sigma_{m,y} \end{bmatrix} \quad (33)$$

820 where $\sigma_{m,x}$ and $\sigma_{m,y}$ is the standard deviation along the x and
821 y axes, respectively. The parameter ρ takes into account the
822 possible inter-dependence of the two coordinates. Independent
823 coordinates have $\rho = 0$.

824 The mean $\boldsymbol{\mu}_n$ depends on the position \mathbf{p}_{n-1} and the speed
825 \mathbf{v}_{n-1} according to

$$826 \quad \boldsymbol{\mu}_n = \mathbf{p}_{n-1} + \mathbf{v}_{n-1}(t_n - t_{n-1}) \quad (34)$$

827 where \mathbf{v}_{n-1} is the vector of the speed along x and y axes at
828 time t_{n-1} .

829 Fig. 12 shows the secrecy map over the surface S as a
830 function of the position of the flasher (22) and with mobility
831 model for the eavesdropper (32). Eve is suspected to move
832 vertically from its previous position, with a mobility model
833 given by (32). The interfering nodes I_1 , I_2 and I_3 are fixed.

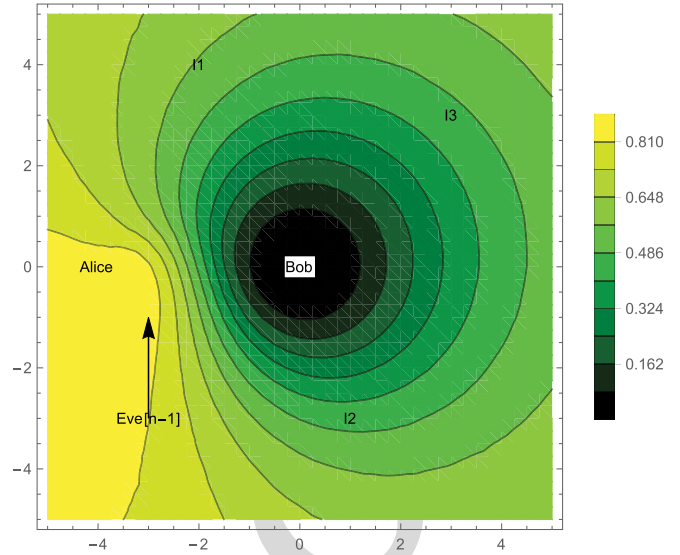


Fig. 12. Secrecy map of the position of the flasher with mobility model for the eavesdropper.

834 Solving (22) gives the optimum point where to locate the
835 additional flasher I_4 . Best is to put the flasher close to the
836 point where the eavesdropper is supposed to arrive. This is
837 somehow trivial.

838 In order to complicate the scenario we supposed that Eve is
839 moving from $(3, -3)$ to $(3, 3)$ with a mobility model given
840 by (32) (see Fig. 13(a)) in six time steps. Alice antenna
841 azimuth orientation can vary from -30 to $+30$ deg. The
842 resulting map of the secrecy pressure is shown in Fig. 13(b).
843 The map shows which is the optimum transmit antenna
844 orientation (azimuth) at each time step. As an example, at
845 time step 6, Eve is stochastically supposed to be in $(3, 3)$
846 and thus an orientation between -18 to $+8$ deg optimizes
847 the secrecy capacity for the Eve's mobility scenario. In this
848 case the secrecy rate achievable is more than 3.20 bps. On the
849 contrary, at time step 3 the maximum secrecy rate achievable is
850 1.28 bps with an antenna orientation range of $(-26, -20)$ deg.

851 VI. SECRECY OUTAGE PROBABILITY 852 OF A SURFACE (SOPS)

853 A closed-form of the secrecy pressure is not easy to be
854 derived. Another interesting metric could be the outage prob-
855 ability of the secrecy capacity over a surface. A secure outage
856 occurs when the instantaneous secrecy capacity $C_{sec}(x, y)$ is
857 less than target secrecy rate \bar{R}_{sec} . Thus, the secure outage
858 probability is defined as

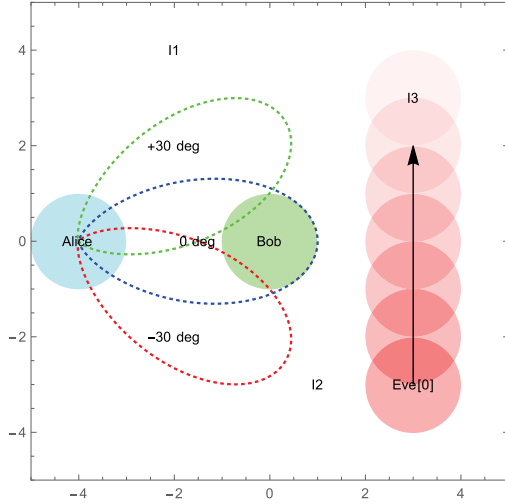
$$859 \quad P_{out}(\bar{R}_{sec})(x, y) = \text{Prob}\{C_{sec}(x, y) < \bar{R}_{sec}\} \quad (35)$$

860 Note that the outage probability depends on the location (x, y)
861 of the eavesdropper over the surface. Given the result above,
862 we define the secrecy outage probability of a surface S (SOPS)
863 as

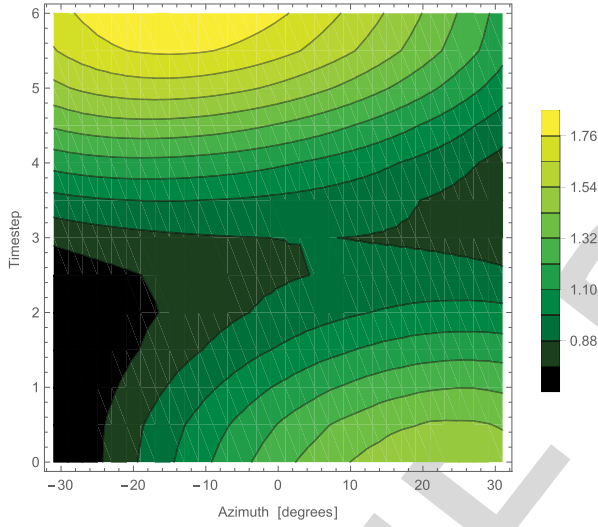
$$864 \quad A_{out}(\bar{R}_{sec}) = \iint_S P_{out}(\bar{R}_{sec})(x, y)v_E(x, y)dxdy$$

$$865 \quad = \iint_S \text{Prob}\{C_{sec}(x, y) < \bar{R}_{sec}\}v_E(x, y)dxdy \quad (36)$$

866



(a) Eve's mobility scenario.



(b) Secrecy map of the Alice's antenna orientation with mobility model for the eavesdropper.

Fig. 13. Eve's mobility: scenario description and secrecy map over azimuth of Alice's antenna.

866 The secrecy outage probability of a surface depends on
 867 the probability $v_E(x, y)$ that Eve is located in the point a
 868 generic point (x, y) of the surface. An interesting behaviour
 869 to study is the existence of the secrecy capacity over a
 870 surface, i.e., when \bar{R}_{sec} is set to zero. In this case the SOPS
 871 becomes

$$872 A_{out}(\bar{R}_{sec} = 0) = \iint_S \text{Prob}\{C_{sec}(x, y) = 0\} v_E(x, y) dx dy$$

873 (37)

874 The term $v_E(x, y)$ is the distribution of the presence of Eve
 875 over the surface, which could be uniform or Gaussian or
 876 any other distribution, based on what it is known about the
 877 eavesdroppers. The term $\text{Prob}\{C_{sec}(x, y) = 0\}$ can be derived
 878 as

$$879 \text{Prob}\{C_{sec}(x, y) = 0\} = \text{Prob}\{SNR_E(x, y) \geq SNR_B\} \quad (38)$$

where

$$SNR_B = \frac{P_B}{N_0 + \mathbf{I}_B} \quad (39)$$

$$SNR_E(x, y) = \frac{P_E}{N_0 + \mathbf{I}_E} \quad (40)$$

with P_B, P_E defined as in (3) and $\mathbf{I}_B, \mathbf{I}_E$ as in (6).
 Eq. (38) is hard to be calculated analytically, since the term
 at numerator P_B is Rayleigh distributed, while the term at
 the denominator \mathbf{I}_B is Stable distributed. A closed form can
 be reached if we assume that the Gaussian approximation is
 valid for the aggregate interference, i.e., $\mathbf{I}_B \sim \mathcal{N}(0, N_B)$ and
 $\mathbf{I}_E \sim \mathcal{N}(0, N_E)$. In this case Eq. (41) becomes

$$SNR_B = \frac{P_B}{N_0 + N_B} \quad (41)$$

$$SNR_E(x, y) = \frac{P_E}{N_0 + N_E} \quad (42)$$

and Eq. (38) can be written as [20]

$$\begin{aligned} \text{Prob}\{C_{sec}(x, y) = 0\} &= \text{Prob}\{SNR_E(x, y) \geq SNR_B\} \\ &= \frac{\overline{SNR}_E(x, y)}{\overline{SNR}_B + \overline{SNR}_E(x, y)} \end{aligned} \quad (43)$$

where

$$\overline{SNR}_i = \frac{\tilde{P}_i d_{A,i}^{-\alpha} \mathbb{E}\{|h_{A,i}|^2\}}{N_0 + N_i}$$

with $i = \{B, E\}$ and $\mathbb{E}\{\cdot\}$ is the expectation operator.

Thus, the SOPS in this case is

$$A_{out}(\bar{R}_{sec} = 0) = \int_x \int_y \frac{\overline{SNR}_E(x, y)}{\overline{SNR}_B + \overline{SNR}_E(x, y)} v_E(x, y) dx dy \quad (44)$$

In the case of a target secrecy rate greater than zero $\bar{R}_{sec} > 0$,
 Eq. (44) is

$$\begin{aligned} A_{out}(\bar{R}_{sec}) &= \iiint_S \text{Prob}\{C_{sec}(x, y) < \bar{R}_{sec}\} v_E(x, y) dx dy \\ &= \int_x \int_y \left(1 - \frac{\overline{SNR}_B \cdot \exp\left\{-\frac{\gamma \bar{R}_{sec}^{-1}}{\overline{SNR}_B}\right\}}{\overline{SNR}_B + 2\bar{R}_{sec} \overline{SNR}_E(x, y)} \right) v_E(x, y) dx dy \end{aligned} \quad (45)$$

The results of the SOPS are shown in Fig. 14. The curves are
 derived by supposing a Gaussian distribution of the presence
 of Eve on the surface, i.e.,

$$v_E(x, y) = \frac{1}{\sqrt{2\sigma_E^2}} e^{-\frac{(x-x_E)^2 + (y-y_E)^2}{2\sigma_E^2}}$$

The other parameters are set as follows: $\mathbb{E}\{|h_{A,i}|^2\} = 1$ with
 $i = \{B, E\}$, σ_E ranges from 0.2 to 5.

Fig. 14 shows the SOPS ($A_{out}(\bar{R}_{sec} = 0)$) as a function of
 the standard deviation σ_E of the distribution of Eve's presence
 on the surface S . Eve is located in three different positions: at
 Alice's, at Bob's and at the first interferer's I_1 . The positions
 of Alice, Bob and the interferers I_1, I_2 and I_3 are shown
 in Fig. 4.

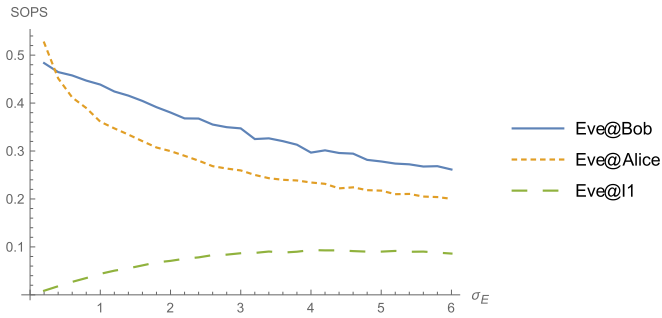


Fig. 14. Secrecy outage of the surface S as a function of the standard deviation σ_E of the distribution of Eve's presence over S . Eve's distribution is Gaussian and centered in three different positions: at Alice's, at Bob's and at the first interferer's I_1 .

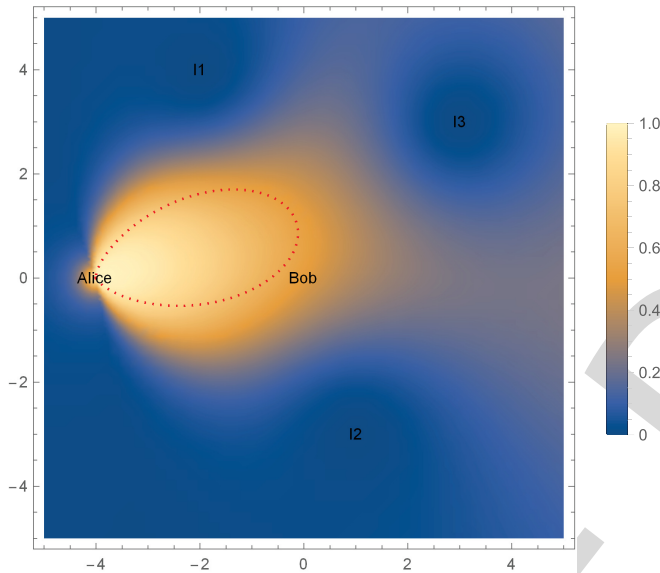


Fig. 15. Secrecy pressure outage map of the surface S .

919 The orange dotted line in Fig. 14 reports the results when
 920 Eve's distribution is centered on the same position of Alice.
 921 The curve of the SOPS confirms that a higher dispersion of the
 922 probability of Eve's presence yields a lower surface secrecy
 923 outage. This is logic, since a higher variance of the Gaussian
 924 distribution means higher probability that Eve is located far
 925 away from Alice. The green dashed line in Fig. 14 reports
 926 the results when Eve's distribution is centered on the same
 927 position of the first interferer I_1 . The curve of the SOPS,
 928 in this case, are completely different from the previous one,
 929 as expected. The SOPS increases with the variance σ_E ,
 930 since a higher dispersion of the position of Eve means a
 931 higher probability that Eve is located far away from the
 932 interference source, which jams Eve's receiver.

933 The blue solid line in Fig. 14 reports the results when
 934 Eve's distribution is centered on Bob's position. The SOPS
 935 increases with the variance σ_E , since a higher dispersion
 936 of the position of Eve means a higher probability that Eve
 937 is located closer to the source of the information (Alice),
 938 i.e., Eve's could have a better signal to noise ratio
 939 compared to Bob.

940 The secrecy pressure outage map of the entire surface is
 941 shown in Fig. 15.

942 VII. CONCLUSIONS

943 This paper proposes and studies a new metric for measuring
 944 the secrecy potentials of a surface. This metric is defined
 945 secrecy pressure. Using the metric different environments or
 946 surfaces can be ordered as a function of the secrecy rate
 947 that can be assured. The metric can be used also for solving
 948 optimization problems, e.g., finding which is the best transmit
 949 antenna orientation to maximize the secrecy capacity of the
 950 surface, or finding which is the best position of an additional
 951 interfering node (friendly jammer). Different practical
 952 scenarios are investigated, including mobility option for the
 953 eavesdropper. Another metric, the secrecy outage probability
 954 of a surface (SOPS), is derived. In this case the presence of
 955 Eve is supposed to be uncertain, and modelled as a Gaussian
 956 distribution over the surface. The results of the SOPS are
 957 shown as a function of the dispersion of Eve's position. The
 958 Gaussian distribution is centered in three specific points: at
 959 Alice's, at Bob's and at the first interferer's.

960 In addition the first part of the paper includes a general
 961 framework to evaluate the secrecy capacity over a surface. The
 962 framework includes all the parameters affecting the secrecy
 963 capacity, from nodes spatial distribution, to antenna orientation
 964 and pattern, and propagation medium statistics.

965 This paper offers a new perspective on the role of secrecy
 966 over a surface, considering nodes spatial distribution, wireless
 967 propagation medium, and aggregate network interference.

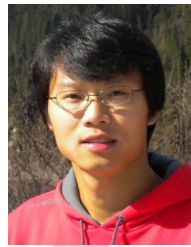
968 REFERENCES

- 969 [1] A. D. Wyner, "The wire-tap channel," *Bell Syst. Tech. J.*, vol. 54, no. 8,
 970 Aug. 1975, p. 13551387.
- 971 [2] S. K. Leung-Yan-Cheong and M. E. Hellman, "The Gaussian wiretap
 972 channel," *IEEE Trans. Inf. Technol. Biomed.*, vol. 24, no. 7, pp. 451–456,
 973 Jul. 1978.
- 974 [3] G. J. Foschini and M. J. Gans, "On limits of wireless communications
 975 in a fading environment when using multiple antennas," *Wireless Pers.
 976 Commun.*, vol. 6, no. 3, pp. 311–335, Mar. 1998.
- 977 [4] Y. Zou, Y.-D. Yao, and B. Zheng, "Opportunistic distributed space-
 978 time coding for decode-and-forward cooperation systems," *IEEE Trans.
 979 Signal Process.*, vol. 60, no. 4, pp. 1766–1781, Apr. 2012.
- 980 [5] S. Lakshmanan, C. L. Tsao, R. Sivakumar, and K. Sundaresan,
 981 "Securing wireless data networks against eavesdropping using smart
 982 antennas, distributed computing systems," in *Proc. IEEE Int.
 983 Conf. Distrib. Comput. Syst. (ICDCS)*, Beijing, China, Jun. 2008,
 984 pp. 19–27.
- 985 [6] Z. Chu, K. Cumanan, Z. Ding, M. Johnston, and S. Y. Le Goff, "Secrecy
 986 rate optimizations for a MIMO secrecy channel with a cooperative
 987 jammer," *IEEE Trans. Veh. Technol.*, vol. 64, no. 5, pp. 1833–1847,
 988 May 2015.
- 989 [7] M. Daly and J. Bernhard, "Directional modulation technique for phased
 990 arrays," *IEEE Trans. Antennas Propag.*, vol. 57, no. 9, pp. 2633–2640,
 991 Sep. 2009.
- 992 [8] M. P. Daly, E. Daly, and J. Bernhard, "Demonstration of directional
 993 modulation using a phased array," *IEEE Trans. Antennas Propag.*,
 994 vol. 58, no. 5, pp. 1545–1550, May 2010.
- 995 [9] A. Kalantari, M. Soltanalian, S. Maleki, S. Chatzinotas, and
 996 B. Ottersten, "Directional modulation via symbol-level precoding: A
 997 way to enhance security," *IEEE J. Sel. Topics Signal Process.*, vol. 16,
 998 no. 8, pp. 1478–1493, Aug. 2016.
- 999 [10] H. Li, X. Wang, and W. Hou, "Security enhancement in cooperative
 1000 jamming using compromised secrecy region minimization," in *Proc. 13th
 1001 Can. Workshop Inf. Theory (CWIT)*, Toronto, ON, Canada, Jun. 2013,
 1002 pp. 214–218.

- 1003 [11] J. Wang, J. Lee, F. Wang, and T. Q. S. Quek, "Jamming-aided secure
1004 communication in massive MIMO Rician channels," *IEEE Trans. Wire-*
1005 *less Commun.*, vol. 14, no. 12, pp. 6854–6868, Dec. 2015.
- 1006 [12] J. M. Carey and D. Grunwald, "Enhancing WLAN security with smart
1007 antennas: A physical layer response for information assurance," in *Proc.*
1008 *Veh. Technol. Conf. (VTC Fall)*, Los Angeles, CA, USA, Sep. 2004,
1009 pp. 318–320.
- 1010 [13] A. Rabbachin, A. Conti, and M. Z. Win, "Wireless network intrinsic
1011 secrecy," *IEEE/ACM Trans. Netw.*, vol. 23, no. 1, pp. 56–69, Feb. 2015.
- 1012 [14] L. Ruan, V. K. N. Lau, and M. Z. Win, "Generalized interference
1013 alignment—Part II: Application to wireless secrecy," *IEEE Trans. Signal*
1014 *Process.*, vol. 64, no. 10, pp. 2688–2701, May 2016.
- 1015 [15] M. Bloch and J. Barros, *Physical-Layer Security: From Information*
1016 *Theory to Security Engineering*. Cambridge, U.K.: Cambridge Univ.
1017 Press, 2011.
- 1018 [16] M. Z. Win, P. C. Pinto, and L. A. Shepp, "A mathematical theory of
1019 network interference and its applications," *Proc. IEEE*, vol. 97, no. 2,
1020 pp. 205–230, Feb. 2009.
- 1021 [17] A. Rabbachin, A. Conti, and M. Z. Win, "The role of aggregate interfer-
1022 ence on intrinsic network secrecy," in *Proc. Int. Conf. Commun. (ICC)*,
1023 Ottawa, ON, Canada, Jun. 2012, pp. 3548–3553.
- 1024 [18] K. I. Pedersen, P. E. Mogensen, and B. H. Fleury, "A stochastic model
1025 of the temporal and azimuthal dispersion seen at the base station in
1026 outdoor propagation environments," *IEEE Trans. Veh. Technol.*, vol. 49,
1027 no. 2, pp. 437–447, Mar. 2000.
- 1028 [19] H. Asplund, A. A. Glazunov, A. F. Molisch, K. I. Pedersen, and
1029 M. Steinbauer, "The COST 259 directional channel model—Part
1030 II: Macrocells," *IEEE Trans. Wireless Commun.*, vol. 5, no. 12,
1031 pp. 3434–3450, Dec. 2006.
- 1032 [20] J. Barros and M. R. D. Rodrigues, "Secrecy capacity of wireless
1033 channels," in *Proc. IEEE Int. Symp. Inf. Theory (ISIT)*, Jul. 2006,
1034 pp. 356–360.



1061 **Luca Ronga** (S'89–M'94–SM'04) received the
1062 M.S. degree in electronic engineering and the Ph.D.
1063 degree in telecommunications from the University
1064 of Florence, Italy, in 1994 and 1998, respectively.
1065 In 1997, he joined as a Visiting Scientist
1066 the International Computer Science Institute of
1067 Berkeley, CA. In 1999, he joined Italian National
1068 Consortium for Telecommunications, where he is
1069 currently heads the research area. He has authored
1070 over 90 papers in international journals and confer-
1071 ence proceedings. His research interests span satel-
1072 lite communications to cognitive radio, software-defined radio, radio resource
1073 management, and wireless security. He has been an Editor of the *EURASIP*
1074 *Newsletter* for four years, a member of the ETSI SatEC Working Group, and
1075 a member of NATO Task Force on Cognitive Radio. He has been a principal
1076 investigator in several research projects.

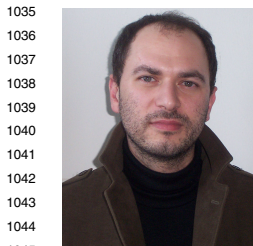


1077 **Xiangyun Zhou** (M'11) received the Ph.D. degree
1078 from The Australian National University (ANU)
1079 in 2010. He is currently a Senior Lecturer with ANU.
1080 His research interests are in the fields of commu-
1081 nication theory and wireless networks. He was a
1082 recipient of the Best Paper Award at at ICC in 2011
1083 and the IEEE ComSoc Asia-Pacific Outstanding
1084 Paper Award in 2016. He served as a Guest Editor
1085 of the *IEEE Communications Magazine* feature topic
1086 on wireless physical layer security in 2015. He has
1087 also served as the symposium, track, and workshop
1088 co-chair for major IEEE conferences. He was the Chair of the ACT Chap-
1089 ter of the IEEE Communications Society and Signal Processing Society
1090 from 2013 to 2014. He currently serves on the Editorial Board of the
1091 IEEE TRANSACTIONS ON WIRELESS COMMUNICATIONS and the IEEE
1092 COMMUNICATIONS LETTERS.



1093 **Kaibin Huang** (M'08–SM'13) received the B.Eng.
1094 degree (Hons.) and the M.Eng. degree from the
1095 National University of Singapore, and the Ph.D.
1096 degree from The University of Texas at Austin
1097 (UT Austin), all in electrical engineering. Since
1098 2014, he has been an Assistant Professor with the
1099 Department of Electrical and Electronic Engineer-
1100 ing (EEE), The University of Hong Kong. He was
1101 a Faculty Member with the Department of Applied
1102 Mathematics (AMA), The Hong Kong Polytechnic
1103 University (PolyU) and the Department of EEE,
1104 Yonsei University, South Korea, where he is currently an Adjunct Professor.

1105 He is also a University Visiting Scholar with Kansai University, Japan.
1106 His research interests focus on the analysis and design of wireless networks
1107 using stochastic geometry, and multi-antenna techniques. He received the
1108 2015 IEEE ComSoc Asia Pacific Outstanding Paper Award, the Outstanding
1109 Teaching Award from Yonsei, the Motorola Partnerships in Research Grant,
1110 the University Continuing Fellowship from UT Austin, and the Best Paper
1111 Award from the IEEE GLOBECOM 2006 and PolyU AMA in 2013. He
1112 frequently serves on the technical program committees of major IEEE
1113 conferences in wireless communications. Most recently, he served as the Lead
1114 Chair of the Wireless Communication Symposium of the IEEE Globecom
1115 2017 and the Communication Theory Symposium of the IEEE GLOBECOM
1116 2014 and the TPC Co-Chair of the IEEE PIMRC 2017 and the IEEE CTW
1117 2013. He was an Editor of the IEEE JOURNAL ON SELECTED AREAS
1118 IN COMMUNICATIONS Series on Green Communications and Networking
1119 from 2015 to 2016, the IEEE WIRELESS COMMUNICATIONS LETTERS
1120 from 2011 to 2016, and the IEEE/KICS JOURNAL OF COMMUNICATION
1121 AND NETWORKS from 2009 to 2015. He edited the IEEE JOURNAL ON
1122 SELECTED AREAS IN COMMUNICATIONS Special Issue on Communications
1123 Powered by Energy Harvesting in 2015. He was an elected member of the
1124 SPCOM Technical Committee of the IEEE Signal Processing Society from
1125 2012 to 2015. He is currently an Editor for the newly established IEEE
1126 TRANSACTIONS ON GREEN COMMUNICATIONS AND NETWORKING, and
1127 the IEEE TRANSACTIONS ON WIRELESS COMMUNICATIONS.

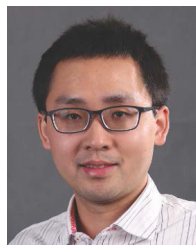


1035 **Lorenzo Mucchi** (M'98–SM'12) received the
1036 Dr.Eng. (Laurea) degree in telecommunications
1037 engineering from the University of Florence, Italy,
1038 in 1998, and the Ph.D. degree in telecommunications
1039 and information society in 2001. Since 2001, he
1040 has been a Research Scientist with the Department
1041 of Information Engineering, University of Florence.
1042 In 2000, he spent a 12 month period of
1043 research at the Center for Wireless Communications,
1044 University of Oulu, Finland. He has been a Pro-
1045 fessor of information technologies with the Univer-
1046 sity of Florence, since 2008. His main research areas include theoretical
1047 modeling, algorithm design, and real measurements, mainly focusing on
1048 physical-layer security, visible light communications, ultra wideband tech-
1049 niques, localization, adaptive diversity techniques, and interference man-
1050 agement. He has authored or co-authored eight book chapters, 32 papers
1051 in international journals, and over 80 papers in international conference
1052 proceedings during his research activity. He was a member of the IEEE
1053 Communications and Information Security Technical Committee in 2009.
1054 Since 2016, he has been an Associate Editor of the IEEE COMMUNICATION
1055 LETTERS. In 2004, he was the Lead Organizer and the General Chair of
1056 the IEEE International Symposium on Medical ICT. He has been the Guest
1057 Editor and the Editor-in-chief of the Elsevier Academic Press Library. He was
1058 a member of the European Telecommunications Standard Institute Smart Body
1059 Area Network (SmartBAN) Group in 2013 and the Team Leader of the special
1060 task force 511 SmartBAN Performance and Coexistence Verification in 2016.



Yifan Chen (M'06–SM'14) received the B.Eng. (Hons.) and Ph.D. degrees in electrical and electronic engineering from Nanyang Technological University, Singapore, in 2002 and 2006, respectively. From 2005 to 2007, he was a Project Officer and then a Research Fellow with the Singapore-University of Washington Alliance in bio-engineering, supported by the Singapore Agency for Science, Technology and Research, Nanyang Technological University, Singapore, and the University of Washington at Seattle, WA, USA. From 2007 to

2012, he was a Lecturer and then a Senior Lecturer with the University of Greenwich and Newcastle University, U.K. From 2012 to 2016, he was a Professor and the Head of Department of Electrical and Electronic Engineering with the Southern University of Science and Technology, Shenzhen, China, appointed through the Recruitment Program of Global Experts (known as the Thousand Talents Plan). In 2013, he was a Visiting Professor with the Singapore University of Technology and Design, Singapore. He is currently a Professor of Engineering and the Associate Dean External Engagement with the Faculty of Science and Engineering and the Faculty of Computing and Mathematical Sciences, University of Waikato, Hamilton, New Zealand. His current research interests include electromagnetic medical imaging and diagnosis, transient communication with application to healthcare, touchable communication and computation with application to targeted drug delivery and contrast-enhanced medical imaging, fundamentals and applications of nanoscale and molecular communications, and channel modeling for next-generation wireless systems and networks. He is the Coordinator of the European FP7 CoNHealth Project on intelligent medical ICT, an elected Working Group Co-leader of the European COST Action TD1301 MiMed Project on microwave medical imaging, an Advisory Committee Member of the European Horizon 2020 CIRCLE Project on molecular communications, a Voting Member of the IEEE Standards Development Working Group 1906.1 on nanoscale and molecular communications, an Editor for the IEEE ComSoc Best Readings in Nanoscale Communication Networks and the IEEE Access Special Section in Nano-antennas, Nano-transceivers, and Nano-networks/Communications, and a Vice Chair of the IEEE Nano-scale, Molecular and Quantum Networking Emerging Technical Subcommittee.



Rui Wang received the bachelor's degree from the University of Science and Technology of China, in 2004, and the Ph.D. degree in wireless communications from The Hong Kong University of Science and Technology, in 2008. From 2009 to 2012, he was a Senior Research Engineer with Huawei Technologies, Co., Ltd. Since 2012, he has been with the South University of Science and Technology of China, as an Associate Professor. He has research experience in academia and industry. He has authored over 30 papers in top-level

IEEE journals and flagship international conferences, especially in the area of wireless radio resource optimization and interference management. He is also involved in the development of interference mitigation technology for 5G systems, and has contributed more than 20 U.S. patent applications and 40 Chinese patent applications (20 of them have been granted).

IEEE PROOF

A New Metric for Measuring the Security of an Environment: The Secrecy Pressure

Lorenzo Mucchi, *Senior Member, IEEE*, Luca Ronga, *Senior Member, IEEE*, Xiangyun Zhou, *Member, IEEE*, Kaibin Huang, *Senior Member, IEEE*, Yifan Chen, *Senior Member, IEEE*, and Rui Wang

Abstract—Information-theoretical approaches can ensure security, regardless of the computational power of the attackers. Requirements for the application of this theory are: 1) assuring an advantage over the eavesdropper quality of reception and 2) knowing where the eavesdropper is. The traditional metrics are the secrecy capacity or outage, which are both related to the quality of the legitimate link against the eavesdropper link. Our goal is to define a new metric, which is the characteristic of the security of the surface/environment where the legitimate link is immersed, regardless of the position of the eavesdropping node. The contribution of this paper is twofold: 1) a general framework for the derivation of the secrecy capacity of a surface, which considers all the parameters that influence the secrecy capacity and 2) the definition of a new metric to measure the secrecy of a surface: the secrecy pressure. The metric can be also visualized as a secrecy map, analogously to weather forecast. Different application scenarios are shown: from “forbidden zone” to Gaussian mobility model for the eavesdropper. Moreover, the secrecy outage probability of a surface is derived. This additional metric can measure, which is the secrecy rate supportable by the specific environment.

Index Terms—Physical-layer security, secrecy pressure, secrecy capacity, secrecy outage, security of wireless communications.

I. INTRODUCTION

IN WIRELESS networks, transmission between legitimate nodes can easily be intercepted by an eavesdropper due to the broadcast nature of the wireless medium. This makes

Manuscript received September 12, 2016; revised January 20, 2017; accepted February 28, 2017. The work of X. Zhou was supported by the Australian Research Council’s Discovery Projects under Grant DP150103905. The work of Y. Chen was supported by the Guangdong Natural Science Funds under Grant 2016A030313640. The associate editor coordinating the review of this paper and approving it for publication was M. Elkashlan.

L. Mucchi is with the Department of Information Engineering, University of Florence, I-50139 Firenze, Italy (e-mail: lorenzo.mucchi@unifi.it).

L. Ronga is with the National Inter-universities Consortium on Telecommunications, University of Firenze research Unit, I-50139 Firenze, Italy (e-mail: luca.ronga@cnit.it).

X. Zhou is with the Research School of Engineering, Australian National University, Canberra, ACT 0200, Australia (e-mail: xiangyun.zhou@anu.edu.au).

K. Huang is with the Department of Electrical and Electronic Engineering, The University of Hong Kong, Hong Kong (e-mail: huangkb@iee.org).

Y. Chen is with the Faculty of Science and Engineering, The University of Waikato, Hamilton 3240, New Zealand, also with the Faculty of Computing and Mathematical Sciences, The University of Waikato, Hamilton 3240, New Zealand, and also with the Department of Electrical and Electronic Engineering, Southern University of Science and Technology, Shenzhen 518055, China (e-mail: yifan.chen@waikato.ac.nz).

R. Wang is with the Department of Electrical and Electronic Engineering, South University of Science and Technology of China, Shenzhen 518055, China (e-mail: wang.r@sustc.edu.cn).

Color versions of one or more of the figures in this paper are available online at <http://ieeexplore.ieee.org>.

Digital Object Identifier 10.1109/TWC.2017.2682245

wireless transmissions highly vulnerable to eavesdropping attacks. Existing communications systems typically adopt cryptographic techniques in order to achieve confidential transmission, to prevent an eavesdropper from interpreting data transmission between legitimate users.

It is known that encrypted transmission is not perfectly secure, since the cipher text can still be decrypted by an eavesdropper through a brute-force attack, an exhaustive search of the encryption key into the cipher text.

To this end, physical-layer security is an emerging alternative paradigm to protect wireless communications against eavesdropping attacks, including brute-force attacks. In fact, the security of cryptographic techniques is implicitly set into the practical assumption that the attacker does not have enough computational power to hack the cipher text in a reasonable amount of time. Thus, security of encryption algorithm cannot be measured exactly. On the contrary, information-theoretical physical-layer security does not need to make any assumption of the computational power of the attacker, and, in addition, the security of a communication link can be exactly measured.

Physical-layer security work was pioneered by Shannon and evolved by Wyner in [1], where a discrete memoryless wiretap channel was examined for secure communications in the presence of an eavesdropper. Perfectly secure data transmission can be achieved if the channel capacity of the legitimate link is higher than the eavesdropper link (from source to eavesdropper). In [2], Wyners results were extended to Gaussian wiretap channel: a new metric, the secrecy capacity, was proposed. The secrecy capacity was derived as the difference between the channel capacity of the legitimate link and of the eavesdropper link. If the secrecy capacity is above zero, the legitimate source can adapt the data rate in order to let the destination decode the information, while the data overheard by the eavesdropper is too few and noisy to be decoded. If the secrecy capacity falls below zero, the transmission from source to destination becomes completely insecure, and the eavesdropper can succeed in interpreting the data. In order to improve the security against eavesdropping attacks, one solution is to reduce the probability of occurrence of an intercept event through enlarging the secrecy capacity.

As a consequence, there are extensive works aimed at increasing the secrecy capacity of wireless communications by exploiting multiple antennas [3] and/or cooperative relays [4].

A. Related Works

There are some examples in literature of papers attempting to create a physical region to face the randomness of the

eavesdropper location and/or the amplitude fluctuation due to fading. All these attempts are basically based on the use of multiple antennas and beamforming [5], [10]–[12]. These works aim at building a region as small as possible where the message can be considered secure. The region is built by using beamforming and/or antenna coding between the legitimate transmitter and receiver, or with the help of friendly surrounding nodes (artificial noise injection, jamming). Actually, the definition of the physical region can differ from paper to paper, but mainly beamforming or jamming are used in the works based on information-theoretical parameters, in the form of antenna arrays [10] or distributed antennas [5].

In [6] secrecy rate maximization and power consumption minimization for a multiple-input multiple-output (MIMO) secrecy channel is investigated. A multiantenna cooperative jammer is employed to improve secret communication in the presence of a multiantenna eavesdropper. In [7] and [8] a phase-shifting array is used to produce security in a given direction (directional modulation). The resulting signal is direction-dependent and thus the signal can be purposely distorted in other directions but the desired one. This approach can be used to enhance the security of multiuser multiple-input multiple output (MIMO) communication systems when a multiantenna eavesdropper is present [9].

The metric used to measure the security of the legitimate link is always the received signal to noise plus interference ratio (SINR) or the secrecy outage. The metric, such as the secrecy outage, is well known in literature and it is related to the quality of the legitimate link, given the position of transmitter and receiver, the transmit parameters (power, coding, beamforming, etc.), as well as the location of eavesdropping nodes and interference sources. Other papers based on information-theoretical security typically use the metrics such as secrecy capacity or secrecy outage to measure the security level of the legitimate link by supposing to know the positions and the channel state information of the eavesdroppers and interferers. In order to drop out the dependence on the positions of the eavesdropping or interference nodes,¹ a more general secrecy metric which is basically a characteristic of the network topology can be reached by averaging out the secrecy capacity over all the possible positions of eavesdroppers or interferers [13], [14]. Anyway, all the above mentioned papers deal with metrics which express a characteristic of the link, not of the surface where the link is immersed.

B. Our Contribution

The secrecy capacity is a good metric to evaluate how much is secure a single communication link. But in many practical scenarios a metric which is related to the specific environment can be more effective. For this reason we propose and test here a new metric which bonds the secrecy to the surface of the environment. We named this metric *secrecy pressure*, taking an analogy from the weather forecasting. The secrecy pressure is defined as the secrecy capacity insisting over the infinitesimal element of the surface. This metric can

be used for several practical scopes: from deriving the secrecy of a specific surface/environment, to calculate which is the optimum transmitting antenna orientation or friendly jammer position.

Differently from traditional metrics such as the conventional secrecy capacity, our metric does not imply to know where Eve is. To be more clear, in our approach the secrecy capacity is calculated for each point (x, y) of a surface S . To do this we suppose that Eve is located in (x, y) . Then, we integrate over x and y along the surface S , thus eliminating the dependence on the position of the eavesdropper. The integration operation is, de facto, as taking the average over the space (instead of time). The resulting metric is the secrecy capacity than the entire surface S has got. We call this metric secrecy pressure since it tells how much security insists over a surface S . In other words, we calculate how much secure is an environment, given the position of Alice, Bob and (if present) interferers. It is more practical because 1) we do not have to make any assumptions on the position of the eavesdropper; 2) the new metric is a property of the environment, and not of the point where Eve is located; 3) we calculate a number which gives an insight on how much secure is the environment were going to transmit. The closest concept to this new metric is the network secrecy developed by M. Win *et al.* [13]. The network secrecy is a metric which evaluates the secrecy of an entire network of nodes (not an environment). Legitimate nodes and eavesdropping nodes are randomly distributed as Poisson point processes (PPP). The secrecy capacity is calculated for each legitimate link, given the position of the eavesdroppers. The dependence on the eavesdroppers positions is dropped by averaging out respect to all possible realization of the PPP distribution of the eavesdropper nodes.

The paper also includes a general framework which evaluates the secrecy capacity over a surface. The framework describes all the parameters affecting the secrecy capacity: spatial distribution of the nodes (legitimate and interfering) on a surface, antennas' orientations and patterns, path loss and fast fading statistics of the communication links, transmitting powers. No hypothesis is made over the position of the eavesdroppers, the metric is calculated over the entire surface, as the eavesdropper could be in each point of the surface. Static as well as statistical mobility model are supposed for the eavesdropper. The results show how the metric can be useful in giving an immediate insight on the leakage zones in the surface, and how to adjust the parameters in order to maximize the secrecy. The optimization problem is here formulated for the transmitting antenna orientation and for the position of a friendly jammer.

It is important to highlight that the secrecy pressure does not need to know the position of the eavesdropper (Eve) on the surface of interest. Typically the papers in literature assume to know the position of Eve, which is usually an unpractical assumption. The secrecy pressure or the secrecy map parameters are calculated by assuming that Eve can stay in each point of the surface. If no information about eavesdropper is known, it could be located in any point of the surface with equal probability. We did not introduce a PPP distribution of eavesdropping nodes, although this is a

¹The eavesdroppers and interferers are supposed to be spatially distributed around the legitimate link with a point poisson process (PPP) distribution.

186 common approach, since we suppose that Eve can stay in each
 187 point of the surface. Typically, the PPP distribution is used
 188 to calculate how many eavesdroppers are within the range of
 189 the legitimate transmitter, and then average out the secrecy
 190 capacity. Our approach is different, we are interested in a
 191 new metric which is a characteristic of the surface. Anyway,
 192 a PPP distribution for the presence of Eve over the surface
 193 can be easily assumed in our case too. The secrecy pressure
 194 contains all the parameters that can cause a variation of the
 195 secrecy capacity, and thus it can be optimized respect to many
 196 (known) parameters (transmit antenna orientation, interference
 197 node positions or powers, etc.), separately or jointly.

198 Another known metric in information-theoretical physical-
 199 layer security is the secrecy outage, i.e., the probability that
 200 the secrecy capacity is below a target rate. We have derived
 201 here the secrecy outage probability of a surface (SOPS). In this
 202 case we have supposed that the presence of Eve on the surface
 203 is not perfectly known, but it has an uncertain which we have
 204 modelled as a Gaussian distribution.

205 The instant fading coefficient of Eve's channel should be
 206 anyway known or estimated in order to derive the secrecy
 207 pressure instant by instant. This estimation can be relaxed
 208 if the evaluation of the secrecy pressure is done in ergodic
 209 channel. The ergodic secrecy pressure can be a useful tool in
 210 many practical applications.

211 Practical applications of the propose metric could be tactical
 212 communications: a scenario in which the transmission cannot
 213 surely be overheard in a particular zone of the surface. Another
 214 scenario could be when the information cannot be leaked along
 215 a specific path or street, where the eavesdropper is supposed
 216 to move.

217 The remainder of this article is organized as follows. Sec. II
 218 describes the system model; the framework for the evaluation
 219 of the secrecy capacity over a surface is introduced, including
 220 all the parameters on which it depends, antenna orientation and
 221 pattern, nodes position and power, etc. In Sec. III, the new
 222 metric called secrecy pressure is defined. Sec. IV proposes
 223 the optimization problems, analytical solutions and graphs.
 224 In Sec. V some practical application scenarios are considered;
 225 antenna orientation as well as friendly jammer problems are
 226 solved in specific scenarios: from forbidden zone to mobility
 227 of the eavesdropper. In Sec. VI the closed-form of the secrecy
 228 outage probability of a surface is derived and discussed.
 229 Sec. VII concludes the paper.

230 II. SYSTEM MODEL

231 Consider a 2D surface S described by Cartesian coordinates
 232 (x, y) . Into this space there are the legitimate transmitter
 233 (node i) and receiver (node j), as well as a given number
 234 of interferers I_k with $k = 1, \dots, N_I$ (Fig. 1). For better
 235 comprehension, let's assume that the space is a geographical
 236 urban area, the transmitter is a base station, the receiver
 237 is a mobile terminal and the interferers are other base
 238 stations or access points. We do not assume any specific
 239 position for the eavesdropper in the space. In fact, we want
 240 to derive how the secrecy is mapped all over the given
 241 environment.

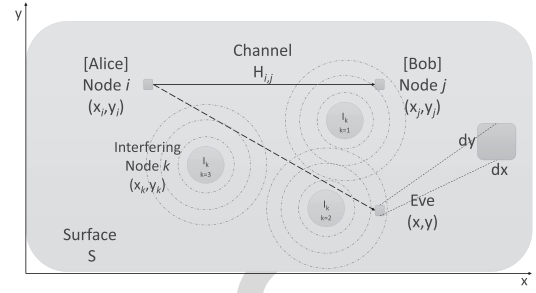


Fig. 1. General scenario. Two legitimate nodes (i and j) want to exchange a confidential message. They are immersed in an environment S together with interfering nodes I_k . The eavesdropper node can be located anywhere over the surface.

242 A. The Scenario

243 We assume to have a surface S where Alice and Bob are
 244 located and their position is known (Fig. 3). In the environ-
 245 ment S there are also interfering nodes, whose positions are
 246 also known. Interfering nodes could be intentional jamming
 247 sources or simply other systems (base stations) radiating in
 248 the same frequency band of the legitimate transmission. To
 249 simulate this scenario, the position of Alice and Bob was
 250 chosen deterministically, while the position of the interfering
 251 nodes were randomly selected, by using a Point Poisson
 252 Process (PPP) distribution. The use of a PPP distribution for
 253 interfering nodes dispersion around a receiver is common in
 254 the literature, when dealing with security of wireless commu-
 255 nications. Alice wants to transmit a confidential message M
 256 to Bob. The legitimate receiver (Bob) tries to recover the message
 257 from the observation vector Z_B . The eavesdropper (Eve) can
 258 be located anywhere in the surface S , and tries to recover
 259 the message M by analyzing the observation vector Z_E . The
 260 wireless channels from Alice to Bob and to Eve are supposed
 261 to be statistically independent.

262 B. Channel Model

263 Let us suppose to have two nodes on the surface S ,
 264 a transmitting node i with position (x_i, y_i) and a receiving
 265 node j with position (x_j, y_j) . The channel between node i
 266 and node j is modeled as

$$267 H_{i,j} = h_{i,j}(\tau, \psi) \cdot d_{i,j}^{-b} \quad (1)$$

268 where $d_{i,j}$ is the Euclidian distance between the nodes, b is
 269 the path loss exponent and $h_{i,j}(\tau, \psi)$ models the multipath
 270 fading effect, including angular dispersion

$$271 h_{i,j}(\tau, \psi) = \sum_{l=1}^L h_{i,j}^{(l)} \delta(\tau - \tau_l) \delta(\psi - \psi_l) \quad (2)$$

272 The parameter τ_l is the delay of arrival of the l -th path, while
 273 ψ_l is the angle of arrival of the l -th path, i.e., τ and ψ
 274 are modeling the time and angular dispersion of the multiple
 275 echoes arriving at the receiver, respectively. The variable
 276 $h_{i,j}^{(l)} = a_{i,j}^{(l)} e^{-\beta_{i,j}^{(l)}}$ denotes the channel coefficient, where $a_{i,j}^{(l)}$
 277 is modelled as a stochastic variable with Rayleigh distribution

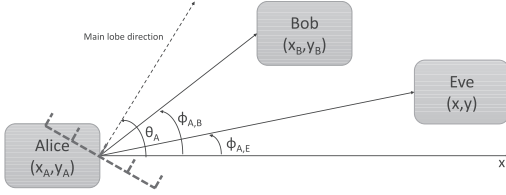


Fig. 2. Antenna pattern of the legitimate transmitter (Alice).

278 whose probability density function (PDF) is

$$279 \quad f_{a_i^{(l)}}(a) = \frac{2a}{\sigma_a} e^{-\frac{a^2}{\sigma_a^2}}$$

280 with σ_a representing the standard deviation of the Rayleigh
 281 distribution, and $\beta_{i,j}^{(l)}$ is modeled as a stochastic random
 282 variable with uniform distribution in $(0, 2\pi)$. Each link that
 283 connect two nodes on the surface is supposed to have a fading
 284 coefficient which is independent to all others.

285 C. Received Power

286 Let us suppose that the node i is transmitting with power P_i .
 287 The power received by the node j is

$$288 \quad P_j = P_i |H_{i,j}|^2 G_i(\theta_i, \phi_{i,j}) G_j(\theta_j, \phi_{j,i}) \quad (3)$$

289 where $G_i(\theta_i, \phi_{i,j})$ is the antenna pattern gain of the
 290 transmitter, $\phi_{i,j}$ is the angle between the x -axis and the
 291 segment connecting node i and j , and θ_i is the angle between
 292 the x -axis and the direction of maximum radiation (main
 293 lobe) of i -node's antenna. Fig. 2 shows the angles mentioned
 294 above, when node i is the legitimate transmitter, called Alice,
 295 and node j is the legitimate receiver, called Bob.

296 Defining $\tilde{P}_{i,j} = P_i G_i(\theta_i, \phi_{i,j}) G_j(\theta_j, \phi_{j,i})$ we can
 297 rewrite (3) as

$$298 \quad P_j = \tilde{P}_{i,j} |H_{i,j}|^2 \quad (4)$$

299 Given the position of node i and j on the surface S , the
 300 angles $\phi_{i,j}$ and $\phi_{j,i}$ are fixed. Then, $\tilde{P}_{i,j} = \tilde{P}_{i,j}(\theta_i, \theta_j)$.
 301 If, in addition, the receiving node j has isotropic antenna
 302 $\theta_j = \text{Const} \forall j$, then $\tilde{P}_{i,j} = \tilde{P}_{i,j}(\theta_i)$.

303 According to [18] and [19], the time dispersion of the
 304 multipath at the receiver has an exponential distribution

$$305 \quad f_\tau(\tau) = \frac{1}{\sigma_\tau} e^{-(\tau-\tau_0)/\sigma_\tau}$$

306 while the angle dispersion of the multipath at the receiver has
 307 a Laplacian distribution

$$308 \quad f_\psi(\psi) = \frac{1}{\sqrt{2\sigma_\psi^2}} e^{-\sqrt{2}(\psi-\psi_0)/\sigma_\psi}$$

309 In order to average out the time and angular dispersion,
 310 the power P_j has to be integrated over all possible times and
 311 angles of arrival

$$312 \quad \bar{P}_j = \tilde{P}_{i,j} d_{i,j}^{-2b} \int_{\tau} \int_{\psi} |h_{i,j}(\tau, \psi)|^2 f_\tau(\tau) f_\psi(\psi) d\tau d\psi \quad (5)$$

D. Aggregate Interference

313 Let us suppose that the N_I interfering nodes are distributed
 314 on the surface S following a point Poisson process (PPP)
 315 distribution with density λ . The sum of the interference power
 316 at the node j is
 317

$$318 \quad \mathbf{I}_j = \sum_{k=1}^{N_I} P_k G_k(\theta_k, \phi_{k,j}) G_j(\theta_j, \phi_{j,k}) d_{k,j}^{-2b} |h_{k,j}|^2$$

$$319 \quad = \sum_k \tilde{P}_{k,j} |H_{k,j}|^2 \quad (6)$$

320 where P_k is the power emitted by the k -th interfering node,
 321 $d_{k,j}$ is the Euclidian distance between the k -th interfering
 322 node and node j and $h_{k,j}$ is the channel coefficient associated
 323 to the link (1). If the position of the N_I interfering nodes
 324 (x_k, y_k) with $k = 1, \dots, N_I$ is fixed, then $\tilde{P}_{k,j} = \tilde{P}_{k,j}(\theta_k, \theta_j)$.
 325 If, in addition, the receiving node j has isotropic antenna
 326 $\theta_j = \text{Const} \forall j$, then $\tilde{P}_{k,j} = \tilde{P}_{k,j}(\theta_k)$. In this case, the
 327 aggregate interference \mathbf{I}_j is a random variable with Stable
 328 distribution [16], [17]

$$329 \quad \mathbf{I}_j \sim S(\alpha, 1, \gamma_j) \quad (7)$$

330 where $\alpha = 1/b$ and

$$331 \quad \gamma_j = \pi \lambda \Xi_\alpha^{-1} \mathbb{E} \left\{ \left(\sum_k \tilde{P}_{k,j} |h_{k,j}|^2 \right)^\alpha \right\}$$

332 with

$$333 \quad \Xi_\alpha = \begin{cases} \frac{1-\alpha}{\Gamma(2-\alpha) \cos(\pi\alpha/2)} & \text{if } \alpha \neq 1 \\ \frac{2}{\pi} & \text{if } \alpha = 1 \end{cases} \quad (8)$$

334 where $\Gamma()$ denotes the Gamma distribution function and $\mathbb{E}\{\}$
 335 the expectation operator.

336 The PDF of \mathbf{I}_j is

$$337 \quad f_{\mathbf{I}_j}(I) = \frac{1}{2\pi} \int \varphi_I(\omega) e^{-j\omega I} d\omega$$

$$338 \quad = \frac{1}{\pi} \int_0^\infty e^{-\omega^\alpha \gamma_j} \cos \left[\tan \left(\frac{\pi\alpha}{2} \right) \omega^\alpha \gamma_j - \omega I \right] d\omega \quad (9)$$

339 where

$$340 \quad \varphi_I(\omega) = \exp \left\{ -|\omega|^\alpha \left[1 - j \text{Sgn}(\omega) \tan \left(\frac{\pi\alpha}{2} \right) \right] \gamma_j \right\}$$

341 is the characteristic function of the random variable I .

342 It is important to highlight that depending on the position
 343 of the receiver j on the surface S , not all the N_I interferers
 344 could affect the receiver. The distance (path loss) $d_{k,j}^{-2b}$
 345 could be close to zero, thus the node k does not contribute to the
 346 aggregate interference at the receiver j .
 347

III. SECRECY PRESSURE AND SECRECY FORCE

348 We want to define a new metric that allows to measure
 349 the intensity of secrecy over a given surface. Taking analogy
 350 from the atmospheric weather science, we define the concept
 351 of *Secrecy Pressure*.
 352

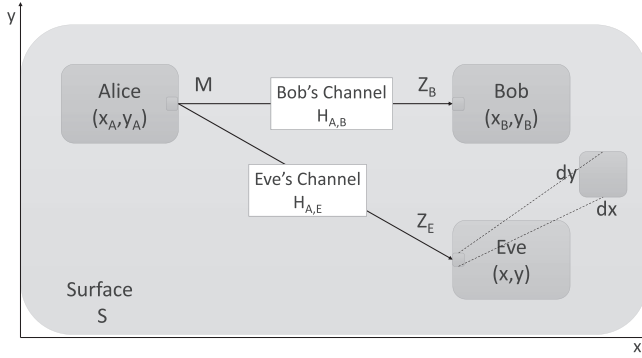


Fig. 3. Scheme of the transmission of the confidential message M from Alice to Bob.

Let us now associate the previous defined transmitting node i as Alice and the receiving node j as Bob. Alice is then located at point (x_A, y_A) and Bob at (x_B, y_B) on the surface S . The position of the eavesdropper Eve is not known, thus we suppose that its coordinates are generically (x, y) .

Suppose that Alice wants to transmit a confidential message M to Bob. Bob tries to recover the information M from the vector Z_B received (Fig. 3). Given the model in Sec. II, the mutual information exchanged in the legitimate link (from Alice to Bob) is

$$\mathbb{I}_B = \mathbb{I}(M; Z_B) = \mathbb{H}(M) - \mathbb{H}(M|Z_B) \quad (10)$$

where $\mathbb{H}()$ denotes the entropy.

Analogously, the eavesdropper (Eve) tries to recover the message M from the received vector Z_E . Thus, the information stolen by Eve is

$$\mathbb{I}_E = \mathbb{I}(M; Z_E) = \mathbb{H}(M) - \mathbb{H}(M|Z_E) \quad (11)$$

The term $\mathbb{I}(M; Z_E)$ is called Leakage, and it denotes the amount of information on the message M that Eve is able to recover from the received vector Z_E .

As known, these two mutual information can be used to calculate the secrecy capacity [15]

$$C_{sec} = \max_{\mathfrak{p}_M} \{\mathbb{I}_B - \mathbb{I}_E\} \geq \max_{\mathfrak{p}_M} \mathbb{I}_B - \max_{\mathfrak{p}_M} \mathbb{I}_E = C_B - C_E \quad (12)$$

where C_B and C_E are the capacities of Bob's and Eve's channel, respectively, and \mathfrak{p}_M is the marginal distribution of the codeword M . The secrecy capacity is at least as large as the difference between the legitimate channel capacity and the eavesdroppers channel capacity. The inequality can be strict as in the case of complex Gaussian wiretap channels [15], as well as typical wireless fading channels, which are here considered. It is important to note that both \mathbb{I}_B and \mathbb{I}_E depend on the channel state and position of Bob and Eve respect to Alice, respectively. This means that changing the position of Bob or Eve on the surface S , the mutual information changes.

The capacity of the link between the transmitter, called Alice, positioned in (x_A, y_A) , and the position (x_B, y_B) of the legitimate receiver, called Bob, can be written as

$$C_B = \frac{1}{2} \log \left(1 + \frac{P_B}{N_0 + \mathbf{I}_B} \right) \quad (13)$$

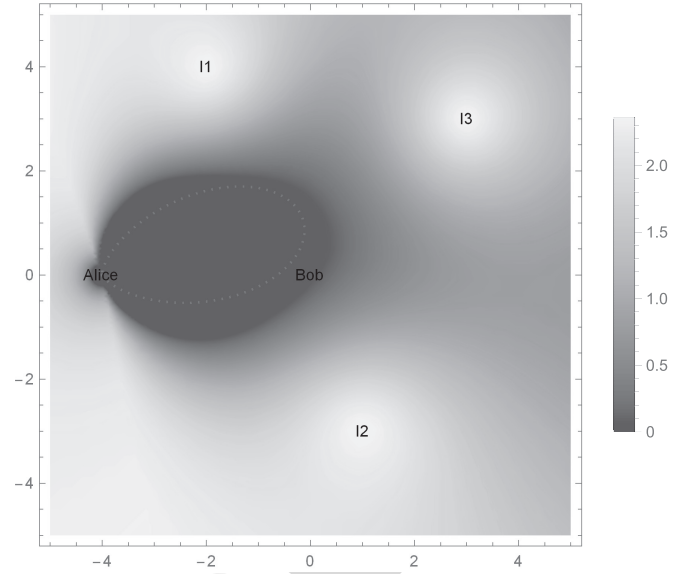


Fig. 4. Secrecy map of surface S with Alice's antenna orientation and pattern. Three interfering nodes (I_1, I_2, I_3) are present. The azimuth of Alice transmission antenna is 6 deg.

where N_0 denotes the Gaussian noise density at the receiver, P_B and \mathbf{I}_B are defined in (4) and (6), respectively.

Since typically we cannot know if an eavesdropper, called Eve, is present in the surface S or where it is located, we derive the capacity of a generic point (x, y) of the surface, i.e.,

$$C_E(x, y) = \frac{1}{2} \log \left(1 + \frac{P_E}{N_0 + \mathbf{I}_E} \right) \quad (14)$$

where P_E and \mathbf{I}_E are defined as in (4) and (6), respectively

$$P_E = P_A G_A(\theta_A, \phi_{A,E}) G_E(\theta_E, \phi_{E,A}) d_{A,E}^{-2b} |h_{A,E}|^2$$

$$\mathbf{I}_E = \sum_{k=1}^{N_I} P_k G_k(\theta_k, \phi_{k,E}) G_E(\theta_E, \phi_{E,k}) d_{k,E}^{-2b} |h_{k,E}|^2$$

Thus, supposing that Eve is located in a generic point (x, y) on the surface S , the secrecy capacity of the link between Alice and Bob is

$$C_{sec}(x, y) = \max\{0, C_B - C_E(x, y)\} = [C_B - C_E(x, y)]^+ \quad (15)$$

It is important to highlight that the capacities here are intended as conditioned to the state of the channels $h_{A,B}$, $h_{A,E}$, $h_{k,B}$ and $h_{k,E}$, as well as the state of the aggregate interference \mathbf{I}_B and \mathbf{I}_E .

What we are proposing here is to define a secrecy capacity for each elementary point (x, y) of the surface S . Using this representation, we can elaborate a map of the secrecy of the surface given the position of the known actors, i.e., legitimate users and interfering nodes. In other words, given the positions of Alice, Bob and interfering nodes I_k , for each point (x, y) of the surface, we calculate the secrecy capacity of the legitimate link as Eve was located in that point. The result is that we can draw a map showing the different levels of secrecy of the entire surface S (Fig. 4).

418 The *Secrecy Pressure* p_{sec} is defined as

$$419 \quad p_{sec} = \frac{1}{A_S} \iint_S C_{sec}(x, y) dx dy = \frac{F_{sec}}{A_S} \quad (16)$$

420 where A_S denotes the area of the surface S and the term F_{sec}
421 is denoting what we define as *Secrecy Force*. The secrecy force
422 depends on the locations of the legitimate users and interfering
423 nodes, but not on the eavesdroppers. The metric p_{sec} is a useful
424 parameter that indicates how much is secure a surface S , given
425 the position of legitimate nodes and interfering nodes. Using
426 this metric, different surfaces and/or nodes configurations can
427 be thus ordered

$$428 \quad p_{sec}^{(1)} < p_{sec}^{(2)} < p_{sec}^{(3)} < \dots$$

429 The index allows a ranking of a given spatial configuration of
430 legitimate entities and interferes.

431 Detailing Eq. (16), we can find an interesting property of
432 the secrecy pressure

$$433 \quad p_{sec} = \frac{1}{A_S} \int_x \int_y \begin{cases} 0 & \text{if } C_B \leq C_E(x, y) \\ C_B - C_E(x, y) & \text{if } C_B > C_E(x, y) \end{cases} dx dy \quad (17)$$

435 Since C_B does not depend on (x, y) , if the surface goes to
436 infinity, the secrecy pressure tends to a constant value

$$437 \quad \lim_{S \rightarrow \infty} p_{sec} = \lim_{S \rightarrow \infty} \left(\frac{1}{A_S} \iint_S [C_B - C_E(x, y)]^+ dx dy \right) = C_B \quad (18)$$

439 This is because the path loss component $d_{A,E}^{-2b}(x, y)$ in (3)
440 vanishes as the generic point (x, y) on the surface S goes
441 to infinity. In practice, the contributions that decrease the
442 secrecy pressure mainly comes from the points on the surface
443 close to the legitimate link. In other words, supposing to
444 have an infinite surface, the set of points where Eve could be
445 located that influence the secrecy capacity is limited, due to
446 the path-loss. A point (x, y) too far away from the legitimate
447 nodes cannot affect the secrecy capacity, since the legitimate
448 signal is received with a too low power to observe anything
449 ($C_E(x, y) = 0$).

450 From Eq. (15) we can derive another useful representation,
451 called *Secrecy Map*. The $C_{sec}(x, y)$ in (15) is indicating
452 which is the secrecy capacity insisting over the elementary
453 unit surface $dx dy$ located in a generic point (x, y) of
454 the surface S (see Fig. 3). This representation can be used to
455 draw the behaviour of the secrecy capacity over the surface S ,
456 showing zones where the secrecy is low or high, analogously
457 to the weather forecast (Fig. 4). The map, in fact, is built by
458 calculating the secrecy capacity of the legitimate link as the
459 eavesdropper was located in each point of the surface. The blue
460 zones in Fig. 4 indicate no secrecy, i.e., if the eavesdropper
461 is set there, the secrecy rate of the legitimate link is zero.
462 Summarizing, the secrecy map is derived by the following
463 steps:

- 464 1) take a surface with cartesian coordinates;
- 465 2) locate the legitimate nodes (Alice and Bob) on the
466 surface;

- 467 3) compute the secrecy capacity of the legitimate link
468 assuming that Eve is located in a point (x, y) of the
469 surface;
- 470 4) associate that secrecy capacity to the corresponding
471 point of the surface;
- 472 5) repeat 3 and 4 for every point of the surface.

473 The secrecy capacity associated to a generic point of the
474 surface could be zero, i.e., any time Eve has a greater channel
475 capacity compared to Bob.

476 The secrecy map of the surface S changes with

- 477 • the positions of Alice, Bob and interfering nodes I_k
478 ($k = 1, \dots, N_I$);
- 479 • the pattern and the orientation $G_A(\theta_A)$ of the legitimate
480 transmitter antenna;
- 481 • the power of the legitimate transmitter P_A ;
- 482 • the power of the transmitters of the interfering nodes P_k ;
- 483 • the state $h_{A,B}$, $h_{A,E}$, $h_{k,B}$ and $h_{k,E}$ of the channels.

484 The effect of time and angle dispersion at the receivers can
485 be averaged out by replacing \bar{P}_j with $j = B$ in (13) and with
486 $j = E$ in (14).

487 As listed in the above items, the secrecy capacity in (15)
488 depends on the instant fading coefficients $h_{A,B}$, $h_{A,E}$, $h_{k,B}$
489 and $h_{k,E}$. This means that the secrecy pressure (16) (and the
490 secrecy map) depends instantly on these processes. In order
491 to remove the dependance on the instantaneous realizations
492 of the fading coefficients, two solutions can be run: 1) put
493 the characteristic function of the fading coefficients into the
494 secrecy capacity formula and average it out, or more easily,
495 2) assume that the channels are ergodic. The results shown
496 in this paper are calculated by supposing ergodic channels.
497 Ergodic-fading model characterizes a situation in which the
498 duration of a coherence interval is on the order of the time
499 required to send a single symbol. The processes $h_{A,B}$, $h_{A,E}$,
500 $h_{k,B}$ and $h_{k,E}$ are mutually independent and i.i.d.; fading coef-
501 ficients change at every channel use and a symbol experiences
502 many fading realizations.

503 The ergodic secrecy capacity is thus [15]

$$504 \quad \tilde{C}_{sec}(x, y) = \mathbb{E}_{|h_{A,B}|^2, |h_{A,E}|^2, |h_{k,B}|^2, |h_{k,E}|^2} \{ [C_B - C_E(x, y)]^+ \} \quad (19)$$

505 $k = 1, \dots, N_I$

506 where the operator $\mathbb{E}\{\}$ stands for the expectation. The ergodic
507 secrecy pressure is obtained by substituting the ergodic secrecy
508 capacity in (19) into Eq. (16)

$$509 \quad \tilde{p}_{sec} = \frac{1}{A_S} \iint_S \tilde{C}_{sec}(x, y) dx dy \quad (20)$$

510 Since $\tilde{C}_{sec}(x, y)$ could be zero in some points of the surface,
511 computing \tilde{p}_{sec} implies to make an integral of an irregular
512 function.

513 It is important to point out that the power received by
514 Eve depends on the position of Eve, since path-loss, fading,
515 angle-of-departure, angle-of-arrival, as well as the power of
516 the aggregate interference are position-dependent parameters.
517 Therefore, in the expression of the capacity of both Bob
518 and Eve, the parameters are position-dependent. Since we
519 want a metric which is not dependent on the position of Eve
520 (its position is not known with 100% probability, typically),

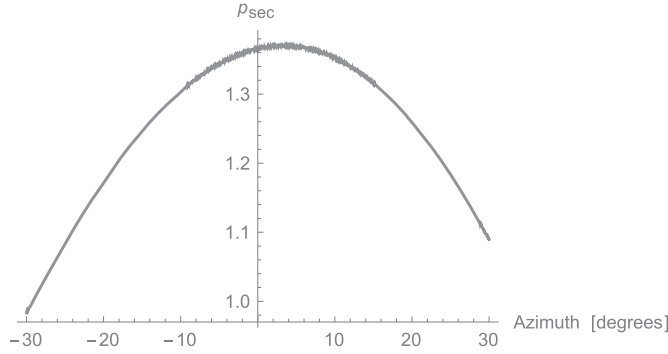


Fig. 5. Secrecy pressure when the optimization problem is solved respect to Alice's antenna orientation.

521 we first locate Eve in each point (x,y) of the surface S , we
 522 calculate the secrecy capacity of each point (x,y) and then we
 523 integrate over the entire surface S . In this way, we take the
 524 mean over a space of the secrecy capacity, which eliminates
 525 the dependence of the secrecy capacity by specific position
 526 of Eve. The resulting (new) metric is a characteristic of the
 527 surface and not of the link, thus we called it secrecy pressure.

528 IV. SECRECY OPTIMIZATION

529 The secrecy pressure can be used as a useful metric to deter-
 530 mine which is the best configuration parameters to optimize
 531 the secrecy of a link. The proposed metric is suitable to find
 532 out different useful results, such as: a) which is the antenna
 533 orientation that assures highest secrecy towards the legitimate
 534 receiver; b) where is the best location where to put additional
 535 interfering node(s) in order to reach higher secrecy for the
 536 legitimate link; c) which is the best configuration of power
 537 emissions from the interfering nodes in order to have highest
 538 secrecy for the legitimate link.

539 A. Antenna Orientation

540 Let us suppose for simplicity that the interfering nodes I_k
 541 as well as Bob and Eve have isotropic antennas. Fixed the
 542 surface S , the positions of the legitimate nodes (Alice, Bob)
 543 and of the interfering nodes I_k ($k = 1, \dots, N_I$), and given the
 544 pattern of the transmitting antenna $G_A(\theta_A)$, we can maximize
 545 the secrecy pressure respect to the antenna orientation

$$546 \quad \arg \max_{\theta_A} \{p_{sec}\} \quad (21)$$

547 Fig. 5 shows the secrecy map over the surface S when
 548 Eve is supposed to be set somewhere in the surface S and
 549 the optimization problem is solved respect to Alice's antenna
 550 orientation. There exists an optimum azimuth orientation of
 551 Alice's antenna. Given the positions of the legitimate users
 552 and interfering nodes, the best, from the secrecy capacity point
 553 of view, for Alice is not to point the maximum of the antenna
 554 pattern towards the direction of Bob. An azimuth orientation of
 555 $+6$ deg optimizes the secrecy capacity, in this case. In general,
 556 with the proposed metric it is possible to derive easily which is
 557 the best antenna orientation for the transmission to a legitimate
 558 receiver in a given perimeter, of which we know only the

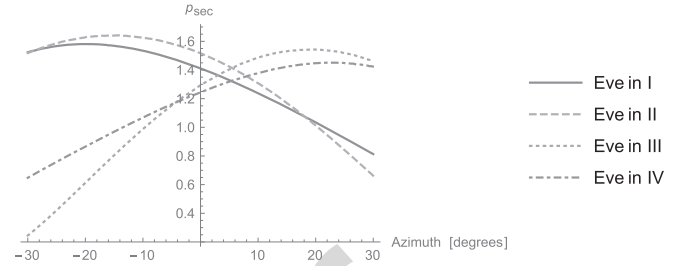


Fig. 6. Secrecy map for different positions of Eve (I, II, III and IV quadrant) when the optimization problem is solved respect to Alice's antenna orientation.

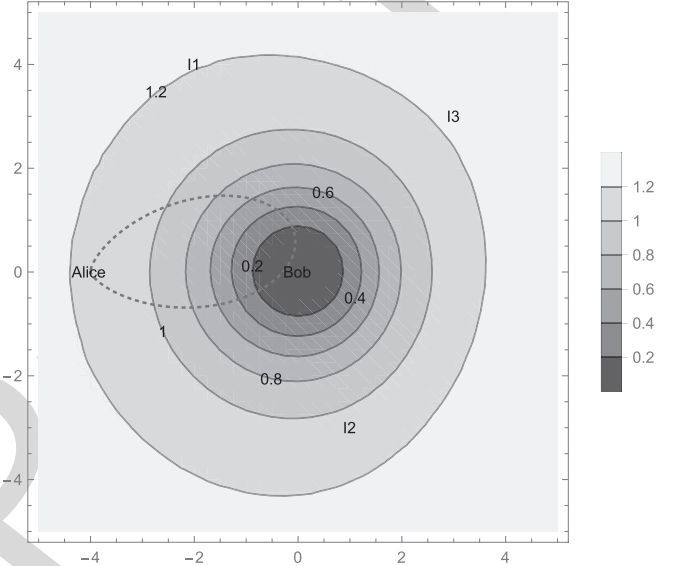


Fig. 7. Secrecy map over the surface S when the optimization problem is solved respect to the position of the additional interfering node (flasher).

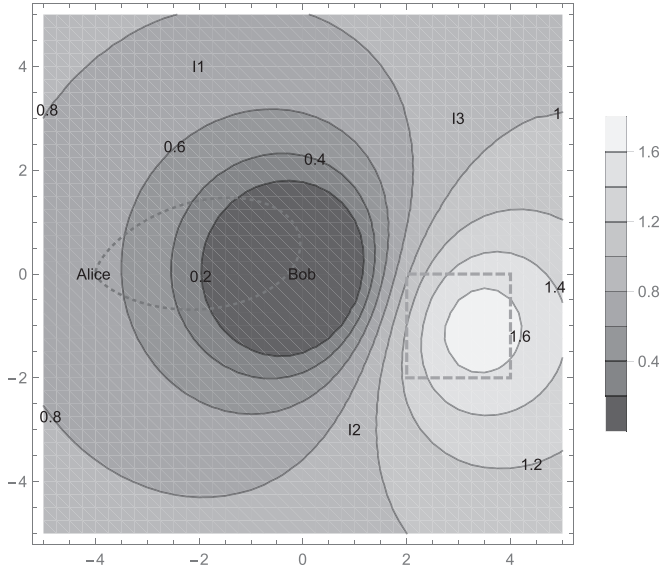
559 positions of the interferers (e.g., other access points or base
 560 stations). Fig. 6 shows the secrecy map over the surface S
 561 for different positions of Eve (I, II, III and IV quadrant)
 562 when the optimization problem is solved respect to Alice's
 563 antenna orientation. As an example, suppose that the legitimate
 564 users do want to minimize the information leakage in a specific
 565 zone of the surface (e.g., the eavesdropper is suspected to be
 566 in the third quadrant), then the optimum antenna orientation
 567 for Alice is $+16$ deg (green curve in Fig. 6).

568 B. Interfering Node Positions

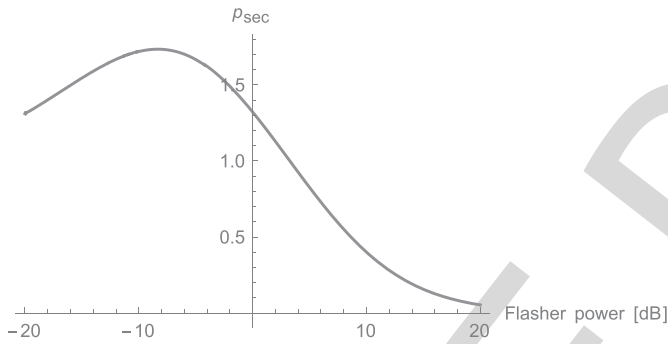
569 Fixed the surface S , the positions of the legitimate nodes
 570 (Alice, Bob) and given the pattern and orientation of the
 571 transmitting antenna $G_A(\theta_A)$, we can maximize the secrecy
 572 pressure over the position (x_k, y_k) of the $N_I + 1$ -th
 573 interfering node, a friendly jammer called here *flasher*, in order
 574 to maximize the secrecy pressure of the legitimate link, given
 575 the positions (fixed) of the N_I interfering nodes

$$576 \quad \arg \max_{(x_k, y_k), k=N_I+1} \{p_{sec}\} \quad (22)$$

577 Fig. 7 shows the secrecy map over the surface S when the
 578 optimization problem (22) is solved. As it can be seen, there
 579 are positions where the additional interference node (flasher)



(a) Secrecy map over the surface S when the optimization problem is solved respect to the position of the additional interfering node (flasher). Eve is supposed to be somewhere in the green dotted line.



(b) Secrecy pressure as a function of the power of the additional interfering node (flasher). The flasher is supposed to be placed in the center of the lighter zone depicted in Fig. 8(a).

Fig. 8. Optimization of both position and power of the additional interfering node (flasher).

580 can be put which optimize the secrecy pressure metric. Like
 581 forecast weather, the areas with same color bring the same
 582 secrecy capacity, if the additional interfering node (friendly
 583 jammer) is installed in that point of the surface. Another
 584 evident result is that the interfering node cannot be placed
 585 close to Bob (white hole in Fig. 7), since the this would
 586 decrease drastically the capacity of the legitimate link and thus
 587 the secrecy capacity. Fig. 8(a) shows the same secrecy map in
 588 the case that Eve is supposed to be somewhere in a limited
 589 perimeter (the green dotted line) inside the surface S . In this
 590 case the optimum area is modified compared to the previous
 591 scenario.

592 C. Power Allocation of the Interferers

593 Fixed the surface S , the positions of the legitimate nodes
 594 (Alice, Bob) and of the interfering nodes² I_k , and given the
 595 pattern and orientation of the transmitting antenna $G_A(\theta_A)$,

²The position of the interfering nodes has been randomly selected by using a PPP distribution.

we can maximize the secrecy pressure respect to the power
 emitted by the interfering nodes

$$\arg \max_{P_k} \{p_{sec}\} \quad k = 1, \dots, N_I \quad (23)$$

To ease the illustration of this optimization, let us suppose
 to put an additional interfering node (the 4th) in the scenario
 and to optimize its transmit power. Figs. 8(a) shows the secrecy
 map over the surface S when the optimization problem is
 solved respect to the position of the additional interfering node
 (flasher) and its power. The eavesdropper is supposed to be
 located somewhere in a limited perimeter (the green dotted line
 in the figure) of the surface. The lighter zone of the secrecy
 map denotes the set of points (x,y) where the flasher can be
 located to yield the highest secrecy pressure. Fig. 8(b) shows
 the secrecy pressure as a function of the power of the flasher.
 The curve evidently shows an optimum point, which in that
 case is about -9 dB.

It is important to stress that using the proposed metric the
 optimum antenna orientation is not trivially in the direction of
 the legitimate receiver, as well as the optimum position and
 power of the intentional jammer (flasher) are not those that
 the common sense would suggest.

D. Joint Optimization

Joint optimization of all the parameters (antenna orientation,
 friendly jammer position and interfering power allocation) is
 also possible

$$\arg \max_{(\theta; (x_k, y_k); P_k)} \{p_{sec}\} \quad k = 1, \dots, N_I \quad (24)$$

Graphical results of this optimization are not shown in this
 paper due to the lack of space.

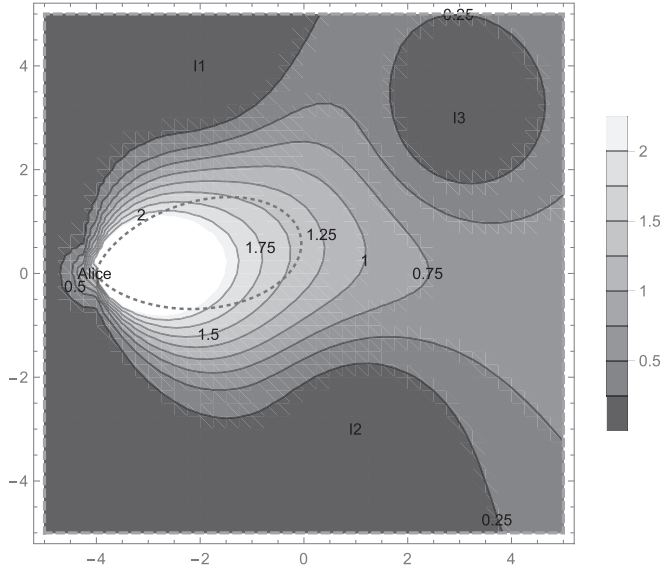
E. Varying the Position of Bob

Although the most practical scenario is when Alice and Bob
 are fixed and Eve can be everywhere in a limited space, as
 previously described, one could also be interested in using the
 proposed metric to draw the map of the secrecy pressure when
 Bob's position can vary over the surface S . In this case, the
 steps to draw the map are the following

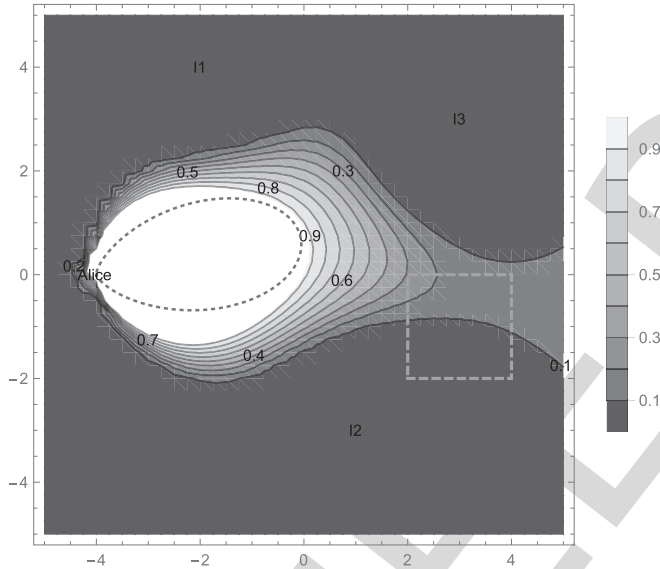
- locate the legitimate receiver (Bob) in a point (x, y) of the surface S ;
- calculate the secrecy pressure metric (20) for Bob located in that point;
- assign to the point (x, y) the value of the secrecy pressure;
- repeat these points until all the surface S is evaluated.

Fig 9(a) shows the map of the secrecy pressure when Bob's
 position varies over the surface and Eve's position varies over
 the entire surface as well. As expected the secrecy pressure is
 higher when Bob is inside the main lobe of Alice, while the
 secrecy pressure decreases drastically when Bob is closer to
 an interferer.

Fig 9(b) shows the map of the secrecy pressure when Bob's
 position vary over the surface and Eve's position varies only
 in a limited perimeter (the green dashed line). Compared to
 Fig 9(a), if Eve is confined into a limited space in



(a) Map of the secrecy pressure as a function of Bob's position. Eve can be everywhere over the surface.



(b) Map of the secrecy pressure as a function of Bob's position. Eve is supposed to be somewhere in the green dotted line.

Fig. 9. Map of the secrecy pressure. The secrecy pressure is calculated as Bob was in each point (x, y) of the surface S .

648 the surface S , the zone of maximum secrecy pressure is larger
 649 and located around the main lobe of Alice. Please note that the
 650 secrecy pressure behind Alice, e.g. the point $(-4, -2)$, is low
 651 since there is almost no power from Alice in that direction.

652 V. GENERAL DEFINITION OF SECRECY PRESSURE 653 AND PRACTICAL APPLICATIONS

654 As stated in the previous sections, the new metric is defined
 655 starting from the definition of the well-known secrecy capacity
 656 (C_{sec}). To eliminate the dependence on the position of the
 657 eavesdropper of the secrecy capacity, we have averaged out
 658 the secrecy capacity by integrating the C_{sec} over the 2D-space
 659 of the specific surface S . The resulting metric is called secrecy

660 pressure and it is the analytical expression of the average over
 661 a space (instead of time). The integral of the C_{sec} function is
 662 not easy to derive, since C_{sec} shows sparsely zeros over the
 663 2D surface, each time that the capacity of Eve is greater of
 664 the capacity of Bob. A closed-form expression of the secrecy
 665 pressure is not easy to obtain, even for simple geometry shape
 666 like circle or square with generic boundaries. For this reason,
 667 we have derived the closed-form expression of the secrecy
 668 outage of a surface (see Sec. VI). Although a closed-form
 669 expression of the secrecy pressure for a known shape is not
 670 shown in the paper, this does not mean that the metric makes
 671 no sense. The metric is defined as the spatial average of the
 672 secrecy capacity calculated for every point of the surface S .
 673 The average of the secrecy capacity over time is called ergodic
 674 secrecy capacity in the literature, but no previous paper, in our
 675 knowledge, presented the spatial average.

676 This metric shows the secrecy as a characteristic of a
 677 surface and not of a single link. This is useful in many
 678 practical scenarios, like military tactical scenarios. Typically,
 679 military command has a specific perimeter of operation, where
 680 the presence of the enemy is not perfectly known, based
 681 on the information that the intelligence service or technolo-
 682 gies (satellite, etc.) can collect. Most probably, the military
 683 command can delimit the presence of the enemy in some
 684 zones of the operational scenario, associating the presence
 685 of the enemy with a certain probability. By calculating the
 686 secrecy pressure, the military command can: 1) quantify how
 687 much secure is one perimeter from the point of view of the
 688 wireless transmissions; 2) decide the optimum angle for the
 689 transmitting antenna array; 3) decide which is the optimum
 690 position to place a jammer to enhance the security of the
 691 transmission; 4) decide the optimum power of the jammer,
 692 in order not to degrade the reception of the legitimate receiver
 693 while jamming the potential eavesdropper; 5) operate a multi-
 694 parameter optimization; 6) if the position of the eavesdropper
 695 is only partially known, the military command can draw
 696 zones in the operational perimeter giving to each of them a
 697 statistical probability of Eve presence, and then compute the
 698 secrecy of the perimeter; 7) if a mobility model of Eve is
 699 known or partially (statistically) known, again all the above
 700 mentioned parameters (antenna orientation, friendly jammer
 701 position, etc.) can be optimized. Other optimizations can be
 702 further imagined.

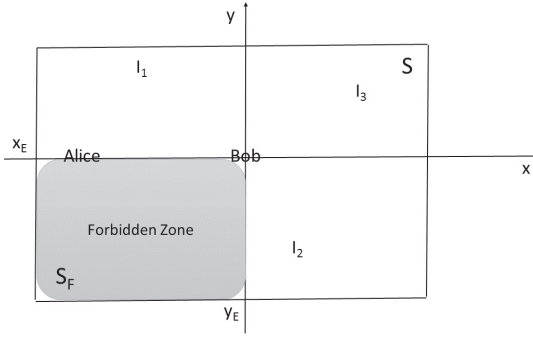
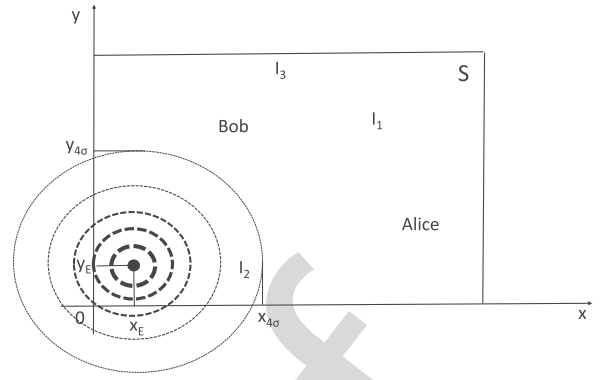
703 As discussed above, in many practical situations we do not
 704 know if an eavesdropper is present and where it is located
 705 exactly. Thus, we define a probability of presence of Eve to
 706 be associated to a generic point (x, y) on the surface S

$$707 \Upsilon_{X,Y}(x, y) = Prob \{x \leq X \leq x + dx, y \leq Y \leq y + dy\} \\
 708 = \int_x^{x+dx} \int_y^{y+dy} v_{X,Y}(x, y) dx dy \quad (25)$$

709 where $v_{X,Y}(x, y)$ is the probability density function (PDF) of
 710 the presence of Eve in (x, y) . From now on we call this PDF
 711 $v_E(x, y)$.

712 The secrecy pressure is thus re-defined as follows

$$713 p_{sec} = \iint_S v_E(x, y) C_{sec}(x, y) dx dy \quad (26)$$

Fig. 10. Forbidden zone inside the surface S .Fig. 11. Gaussian distribution of Eve's presence inside the surface S .

714 where $C_{sec}(x, y) = [C_B - C_E(x, y)]^+$ and $\iint v_E(x, y)$
 715 $dx dy = 1$. Eq. (26) represents the more general expression
 716 of the secrecy pressure in (16). For example, if a uniform
 717 distribution of Eve's presence is supposed for the entire
 718 surface S , the PDF would be $v_E(x, y) = 1/A_S$ and thus
 719 $\iint_S 1/A_S dx dy = 1$.

720 In the following sections three practical scenarios are pro-
 721 posed to show the benefits of the new proposed metric.
 722 In particular, the secrecy pressure is computed when

- 723 • an eavesdropper is known to be in a sub-region of the
- 724 surface S (leakage zone),
- 725 • the eavesdropper position is known with a probability
- 726 spatial function (Gaussian approximation), and
- 727 • when the eavesdropper has not a fixed position (mobility
- 728 scenario).

729 In all these cases, some simplifications are assumed

- 730 • the average fading of the channels is supposed to be 1,
- 731 i.e., $\sum_l |h_{i,j}^{(l)}|^2 = 1$;
- 732 • the antenna pattern of Bob, Eve and of the interfering
- 733 nodes is supposed to be isotropic. Only Alice has a
- 734 directive antenna and can modify the antenna orientation;
- 735 • the position of Alice and Bob on the surface S is supposed
- 736 to be fixed and known: $(-4, 0)$ and $(0, 0)$, respectively;
- 737 • the position of the interfering nodes (I_1, I_2, I_3) is supposed
- 738 to be fixed and known: $(-2, 4)$, $(1, -3)$ and $(3, 3)$,
- 739 respectively.

740 A. Leakage Zone

741 In many real situations, e.g., in military scenarios, the
 742 transmitter does not want to leak information in fixed zone,
 743 in a region where it knows that an eavesdropper is surely
 744 present. We name here the leakage zone as *forbidden zone*,
 745 since the legitimate transmitter surely does not want to leak
 746 any information in that zone. Fig. 10 shows the surface S with
 747 the forbidden zone S_F inside. In this example the forbidden
 748 zone is the third quadrant.

749 To each point of the surface S_F we associate a probability
 750 of Eve's presence such that $\iint_{S_F} v_E(S) dx dy = 1$, while in
 751 the rest of the surface S we set $\iint_{-S_F} v_E(S) dx dy = 0$, where
 752 $-S_F$ denotes the complementary surface $S_F \cup -S_F = S$.

753 Assume, as an example, to have an equal distribution
 754 of the probability of Eve's presence in the surface S_F .

755 Than,

$$756 v_E(x, y) = \begin{cases} \frac{1}{x_E y_E}, & \text{if } x \in [0, x_E] \text{ and } y \in [0, y_E] \\ 0, & \text{otherwise} \end{cases} \quad (27)$$

757 In this case the secrecy pressure of the surface (26) is

$$758 p_{sec} = \int_0^{x_E} \int_0^{y_E} v_E(x, y) C_{sec}(x, y) dx dy \quad (28)$$

759 The secrecy map of the surface can be drawn by using the
 760 following result

$$761 v_E(x, y) C_{sec}(x, y) = \begin{cases} 0 & \text{if } C_{sec}(x, y) = 0 \\ C_B - \frac{1}{x_E y_E} \int_0^{x_E} \int_0^{y_E} C_E(x, y) dx dy & \text{otherwise} \end{cases} \quad (29)$$

764 The optimization of the secrecy pressure respect to the
 765 azimuth of the transmitting antenna of the legitimate node
 766 (Alice) for a forbidden zone is shown in Fig. 5.

767 B. Gaussian Probability of Eavesdropper Presence

768 In other situations, it is not known exactly if eavesdroppers
 769 are present or not. Only suspicious. In this case, located a
 770 point on the map, a probability of presence of Eve with
 771 certain distribution can be associated. We suppose here that
 772 a Gaussian spatial distribution of Eve's presence is associated
 773 to a zone of the surface S . To each point of the surface
 774 S we associate a probability of Eve's presence v_E which
 775 is a random variable with Gaussian distribution centered in
 776 (x_E, y_E) (Fig. 11). The circle lines denotes the intensity of
 777 the probability. For example, if the Gaussian random variable
 778 denoting the presence of Eve on the surface has mean 0.8 and
 779 variance 1, we associate a probability of Eve's presence equal
 780 to 0.8 to the point (x_E, y_E) .

781 In this case the secrecy pressure of the surface (26) is

$$782 p_{sec} = \iint_S v_E(x, y) C_{sec}(x, y) dx dy \quad (30)$$

783 With $v_E(x, y) = \frac{1}{\sqrt{2\sigma_E^2}} e^{-\frac{(x-x_E)^2 + (y-y_E)^2}{2\sigma_E^2}}$, where σ_E indicates the
 784 standard deviation of the Gaussian distribution.

The secrecy map of the surface can be drawn by using the following result

$$v_E(x, y)C_{sec}(x, y)dxdy = \begin{cases} 0 & \text{if } C_{sec}(x, y) \leq 0 \\ C_B - \iint_S v_E(x, y)C_E(x, y)dxdy & \text{otherwise} \end{cases} \quad (31)$$

This scenario is a particular case of the mobility scenario described in the next section, the results can be appreciated in Fig. 13(b).

C. Mobility Model for the Eavesdropper

If we know the position of Eve at time t_n , we can associate to the eavesdropper a statistical mobility model and derive the secrecy pressure over a surface of interest. The mobility model for Eve depends on its movement capability in the specific environment. In the absence of prior information on the real movement of the eavesdropper (i.e., Eve is free to move in all directions with different speeds), the Gaussian mobility model represents a fairly general model with a tractable number of parameters. In the presence of some prior information on the eavesdroppers movement (e.g., direction or speed is set by the environment), a mobility model more tight to the real mobility would provide better performance.

Optimization of the secrecy pressure is shown respect to the azimuth of the legitimate transmitting antenna as well as respect to the position of the flasher.

We consider here Gaussian mobility model with conditional PDF of current position conditioned on the previous position. For easier notation, let us define the position (x, y) at time t_n of a point on the surface S as a vector \mathbf{p}_n . Thus, the conditional PDF of current position is

$$v_m(\mathbf{p}_n|\mathbf{p}_{n-1}) = \frac{1}{2\pi|\Sigma_m|^{\frac{1}{2}}} e^{-\frac{1}{2}[(\mathbf{p}_n - \boldsymbol{\mu}_n)^T \Sigma_m^{-1}(\mathbf{p}_n - \boldsymbol{\mu}_n)]} \quad (32)$$

where $\boldsymbol{\mu}_n$ varies with the mobility model as described in the following, and the covariance matrix Σ_m accounts for the uncertainty in the movements in a 2-D plane; thus, it is expressed by

$$\Sigma_m = \begin{bmatrix} \sigma_{m,x} & \rho\sigma_{m,x}\sigma_{m,y} \\ \rho\sigma_{m,x}\sigma_{m,y} & \sigma_{m,y} \end{bmatrix} \quad (33)$$

where $\sigma_{m,x}$ and $\sigma_{m,y}$ is the standard deviation along the x and y axes, respectively. The parameter ρ takes into account the possible inter-dependence of the two coordinates. Independent coordinates have $\rho = 0$.

The mean $\boldsymbol{\mu}_n$ depends on the position \mathbf{p}_{n-1} and the speed \mathbf{v}_{n-1} according to

$$\boldsymbol{\mu}_n = \mathbf{p}_{n-1} + \mathbf{v}_{n-1}(t_n - t_{n-1}) \quad (34)$$

where \mathbf{v}_{n-1} is the vector of the speed along x and y axes at time t_{n-1} .

Fig. 12 shows the secrecy map over the surface S as a function of the position of the flasher (22) and with mobility model for the eavesdropper (32). Eve is suspected to move vertically from its previous position, with a mobility model given by (32). The interfering nodes I_1 , I_2 and I_3 are fixed.

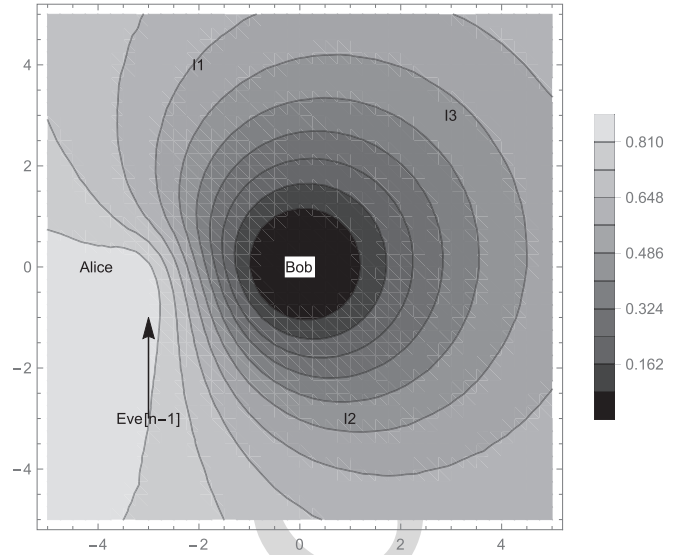


Fig. 12. Secrecy map of the position of the flasher with mobility model for the eavesdropper.

Solving (22) gives the optimum point where to locate the additional flasher I_4 . Best is to put the flasher close to the point where the eavesdropper is supposed to arrive. This is somehow trivial.

In order to complicate the scenario we supposed that Eve is moving from $(3, -3)$ to $(3, 3)$ with a mobility model given by (32) (see Fig. 13(a)) in six time steps. Alice antenna azimuth orientation can vary from -30 to $+30$ deg. The resulting map of the secrecy pressure is shown in Fig. 13(b). The map shows which is the optimum transmit antenna orientation (azimuth) at each time step. As an example, at time step 6, Eve is stochastically supposed to be in $(3, 3)$ and thus an orientation between -18 to $+8$ deg optimizes the secrecy capacity for the Eve's mobility scenario. In this case the secrecy rate achievable is more than 3.20 bps. On the contrary, at time step 3 the maximum secrecy rate achievable is 1.28 bps with an antenna orientation range of $(-26, -20)$ deg.

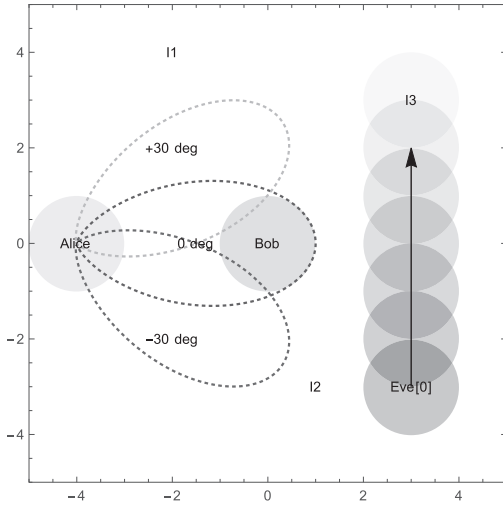
VI. SECRECY OUTAGE PROBABILITY OF A SURFACE (SOPS)

A closed-form of the secrecy pressure is not easy to be derived. Another interesting metric could be the outage probability of the secrecy capacity over a surface. A secure outage occurs when the instantaneous secrecy capacity $C_{sec}(x, y)$ is less than target secrecy rate \bar{R}_{sec} . Thus, the secure outage probability is defined as

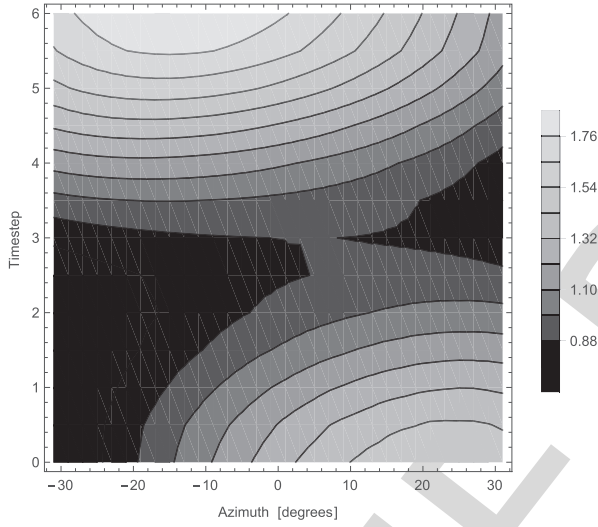
$$P_{out}(\bar{R}_{sec})(x, y) = \text{Prob}\{C_{sec}(x, y) < \bar{R}_{sec}\} \quad (35)$$

Note that the outage probability depends on the location (x, y) of the eavesdropper over the surface. Given the result above, we define the secrecy outage probability of a surface S (SOPS) as

$$A_{out}(\bar{R}_{sec}) = \iint_S P_{out}(\bar{R}_{sec})(x, y)v_E(x, y)dxdy = \iint_S \text{Prob}\{C_{sec}(x, y) < \bar{R}_{sec}\}v_E(x, y)dxdy \quad (36)$$



(a) Eve's mobility scenario.



(b) Secrecy map of the Alice's antenna orientation with mobility model for the eavesdropper.

Fig. 13. Eve's mobility: scenario description and secrecy map over azimuth of Alice's antenna.

866 The secrecy outage probability of a surface depends on
 867 the probability $v_E(x, y)$ that Eve is located in the point a
 868 generic point (x, y) of the surface. An interesting behaviour
 869 to study is the existence of the secrecy capacity over a
 870 surface, i.e., when \bar{R}_{sec} is set to zero. In this case the SOPS
 871 becomes

$$872 A_{out}(\bar{R}_{sec} = 0) = \iint_S \text{Prob}\{C_{sec}(x, y) = 0\} v_E(x, y) dx dy$$

873 (37)

874 The term $v_E(x, y)$ is the distribution of the presence of Eve
 875 over the surface, which could be uniform or Gaussian or
 876 any other distribution, based on what it is known about the
 877 eavesdroppers. The term $\text{Prob}\{C_{sec}(x, y) = 0\}$ can be derived
 878 as

$$879 \text{Prob}\{C_{sec}(x, y) = 0\} = \text{Prob}\{SNR_E(x, y) \geq SNR_B\} \quad (38)$$

where

$$SNR_B = \frac{P_B}{N_0 + \mathbf{I}_B} \quad (39)$$

$$SNR_E(x, y) = \frac{P_E}{N_0 + \mathbf{I}_E} \quad (40)$$

with P_B , P_E defined as in (3) and \mathbf{I}_B , \mathbf{I}_E as in (6).
 Eq. (38) is hard to be calculated analytically, since the term
 at numerator P_B is Rayleigh distributed, while the term
 at the denominator \mathbf{I}_B is Stable distributed. A closed form can
 be reached if we assume that the Gaussian approximation is
 valid for the aggregate interference, i.e., $\mathbf{I}_B \sim \mathcal{N}(0, N_B)$ and
 $\mathbf{I}_E \sim \mathcal{N}(0, N_E)$. In this case Eq. (41) becomes

$$SNR_B = \frac{P_B}{N_0 + N_B} \quad (41)$$

$$SNR_E(x, y) = \frac{P_E}{N_0 + N_E} \quad (42)$$

and Eq. (38) can be written as [20]

$$\begin{aligned} \text{Prob}\{C_{sec}(x, y) = 0\} &= \text{Prob}\{SNR_E(x, y) \geq SNR_B\} \\ &= \frac{\overline{SNR}_E(x, y)}{\overline{SNR}_B + \overline{SNR}_E(x, y)} \end{aligned} \quad (43)$$

where

$$\overline{SNR}_i = \frac{\tilde{P}_i d_{A,i}^{-b} \mathbb{E}\{|h_{A,i}|^2\}}{N_0 + N_i}$$

with $i = \{B, E\}$ and $\mathbb{E}\{\}$ is the expectation operator.

Thus, the SOPS in this case is

$$A_{out}(\bar{R}_{sec} = 0) = \int_x \int_y \frac{\overline{SNR}_E(x, y)}{\overline{SNR}_B + \overline{SNR}_E(x, y)} v_E(x, y) dx dy \quad (44)$$

In the case of a target secrecy rate greater than zero $\bar{R}_{sec} > 0$,
 Eq. (44) is

$$\begin{aligned} A_{out}(\bar{R}_{sec}) &= \iiint_S \text{Prob}\{C_{sec}(x, y) < \bar{R}_{sec}\} v_E(x, y) dx dy \\ &= \int_x \int_y \left(1 - \frac{\overline{SNR}_B \cdot \exp\left\{-\frac{2\bar{R}_{sec}-1}{\overline{SNR}_B}\right\}}{\overline{SNR}_B + 2\bar{R}_{sec} \overline{SNR}_E(x, y)} \right) v_E(x, y) dx dy \end{aligned} \quad (45)$$

The results of the SOPS are shown in Fig. 14. The curves are
 derived by supposing a Gaussian distribution of the presence
 of Eve on the surface, i.e.,

$$v_E(x, y) = \frac{1}{\sqrt{2\sigma_E^2}} e^{-\frac{(x-x_E)^2 + (y-y_E)^2}{2\sigma_E^2}}$$

The other parameters are set as follows: $\mathbb{E}\{|h_{A,i}|^2\} = 1$ with
 $i = \{B, E\}$, σ_E ranges from 0.2 to 5.

Fig. 14 shows the SOPS ($A_{out}(\bar{R}_{sec} = 0)$) as a function of
 the standard deviation σ_E of the distribution of Eve's presence
 on the surface S . Eve is located in three different positions: at
 Alice's, at Bob's and at the first interferer's I_1 . The positions
 of Alice, Bob and the interferers I_1 , I_2 and I_3 are shown
 in Fig. 4.

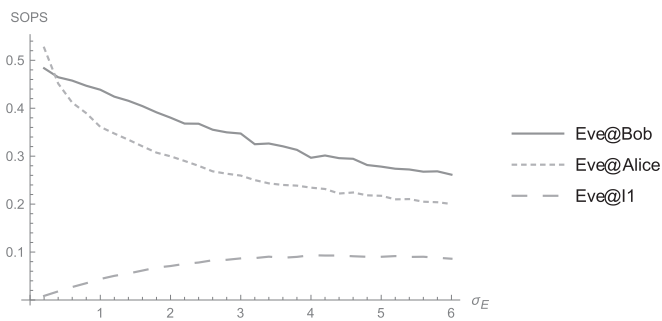


Fig. 14. Secrecy outage of the surface S as a function of the standard deviation σ_E of the distribution of Eve's presence over S . Eve's distribution is Gaussian and centered in three different positions: at Alice's, at Bob's and at the first interferer's I_1 .

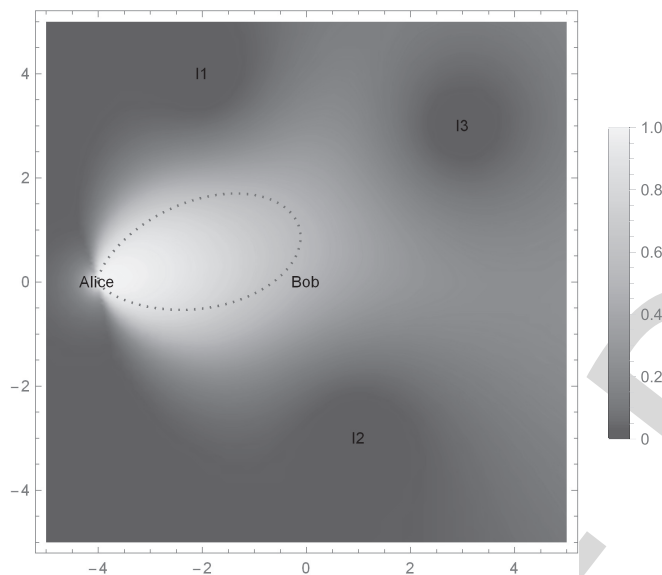


Fig. 15. Secrecy pressure outage map of the surface S .

919 The orange dotted line in Fig. 14 reports the results when
 920 Eve's distribution is centered on the same position of Alice.
 921 The curve of the SOPS confirms that a higher dispersion of the
 922 probability of Eve's presence yields a lower surface secrecy
 923 outage. This is logic, since a higher variance of the Gaussian
 924 distribution means higher probability that Eve is located far
 925 away from Alice. The green dashed line in Fig. 14 reports
 926 the results when Eve's distribution is centered on the same
 927 position of the first interferer I_1 . The curve of the SOPS, in
 928 this case, are completely different from the previous one, as
 929 expected. The SOPS increases with the variance σ_E , since
 930 a higher dispersion of the position of Eve means a higher
 931 probability that Eve is located far away from the interference
 932 source, which jams Eve's receiver.

933 The blue solid line in Fig. 14 reports the results when
 934 Eve's distribution is centered on Bob's position. The SOPS
 935 increases with the variance σ_E , since a higher dispersion of
 936 the position of Eve means a higher probability that Eve is
 937 located closer to the source of the information (Alice), i.e.,
 938 Eve's could have a better signal to noise ratio compared
 939 to Bob.

940 The secrecy pressure outage map of the entire surface is
 941 shown in Fig. 15.

942 VII. CONCLUSIONS

943 This paper proposes and studies a new metric for measuring
 944 the secrecy potentials of a surface. This metric is defined
 945 secrecy pressure. Using the metric different environments or
 946 surfaces can be ordered as a function of the secrecy rate
 947 that can be assured. The metric can be used also for solving
 948 optimization problems, e.g., finding which is the best transmit
 949 antenna orientation to maximize the secrecy capacity of the
 950 surface, or finding which is the best position of an additional
 951 interfering node (friendly jammer). Different practical
 952 scenarios are investigated, including mobility option for the
 953 eavesdropper. Another metric, the secrecy outage probability
 954 of a surface (SOPS), is derived. In this case the presence of
 955 Eve is supposed to be uncertain, and modelled as a Gaussian
 956 distribution over the surface. The results of the SOPS are
 957 shown as a function of the dispersion of Eve's position. The
 958 Gaussian distribution is centered in three specific points: at
 959 Alice's, at Bob's and at the first interferer's.

960 In addition the first part of the paper includes a general
 961 framework to evaluate the secrecy capacity over a surface. The
 962 framework includes all the parameters affecting the secrecy
 963 capacity, from nodes spatial distribution, to antenna orientation
 964 and pattern, and propagation medium statistics.

965 This paper offers a new perspective on the role of secrecy
 966 over a surface, considering nodes spatial distribution, wireless
 967 propagation medium, and aggregate network interference.

968 REFERENCES

- 969 [1] A. D. Wyner, "The wire-tap channel," *Bell Syst. Tech. J.*, vol. 54, no. 8,
 970 Aug. 1975, p. 13551387.
- 971 [2] S. K. Leung-Yan-Cheong and M. E. Hellman, "The Gaussian wiretap
 972 channel," *IEEE Trans. Inf. Technol. Biomed.*, vol. 24, no. 7, pp. 451–456,
 973 Jul. 1978.
- 974 [3] G. J. Foschini and M. J. Gans, "On limits of wireless communications
 975 in a fading environment when using multiple antennas," *Wireless Pers.*
 976 *Commun.*, vol. 6, no. 3, pp. 311–335, Mar. 1998.
- 977 [4] Y. Zou, Y.-D. Yao, and B. Zheng, "Opportunistic distributed space-
 978 time coding for decode-and-forward cooperation systems," *IEEE Trans.*
 979 *Signal Process.*, vol. 60, no. 4, pp. 1766–1781, Apr. 2012.
- 980 [5] S. Lakshmanan, C. L. Tsao, R. Sivakumar, and K. Sundaresan,
 981 "Securing wireless data networks against eavesdropping using smart
 982 antennas, distributed computing systems," in *Proc. IEEE Int.*
 983 *Conf. Distrib. Comput. Syst. (ICDCS)*, Beijing, China, Jun. 2008,
 984 pp. 19–27.
- 985 [6] Z. Chu, K. Cumanan, Z. Ding, M. Johnston, and S. Y. Le Goff, "Secrecy
 986 rate optimizations for a MIMO secrecy channel with a cooperative
 987 jammer," *IEEE Trans. Veh. Technol.*, vol. 64, no. 5, pp. 1833–1847,
 988 May 2015.
- 989 [7] M. Daly and J. Bernhard, "Directional modulation technique for phased
 990 arrays," *IEEE Trans. Antennas Propag.*, vol. 57, no. 9, pp. 2633–2640,
 991 Sep. 2009.
- 992 [8] M. P. Daly, E. Daly, and J. Bernhard, "Demonstration of directional
 993 modulation using a phased array," *IEEE Trans. Antennas Propag.*,
 994 vol. 58, no. 5, pp. 1545–1550, May 2010.
- 995 [9] A. Kalantari, M. Soltanalian, S. Maleki, S. Chatzinotas, and
 996 B. Ottersten, "Directional modulation via symbol-level precoding: A
 997 way to enhance security," *IEEE J. Sel. Topics Signal Process.*, vol. 16,
 998 no. 8, pp. 1478–1493, Aug. 2016.
- 999 [10] H. Li, X. Wang, and W. Hou, "Security enhancement in cooperative
 1000 jamming using compromised secrecy region minimization," in *Proc. 13th*
 1001 *Can. Workshop Inf. Theory (CWIT)*, Toronto, ON, Canada, Jun. 2013,
 1002 pp. 214–218.

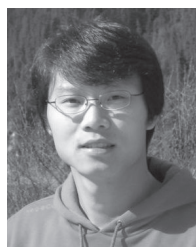
- 1003 [11] J. Wang, J. Lee, F. Wang, and T. Q. S. Quek, "Jamming-aided secure
1004 communication in massive MIMO Rician channels," *IEEE Trans. Wire-*
1005 *less Commun.*, vol. 14, no. 12, pp. 6854–6868, Dec. 2015.
- 1006 [12] J. M. Carey and D. Grunwald, "Enhancing WLAN security with smart
1007 antennas: A physical layer response for information assurance," in *Proc.*
1008 *Veh. Technol. Conf. (VTC Fall)*, Los Angeles, CA, USA, Sep. 2004,
1009 pp. 318–320.
- 1010 [13] A. Rabbachin, A. Conti, and M. Z. Win, "Wireless network intrinsic
1011 secrecy," *IEEE/ACM Trans. Netw.*, vol. 23, no. 1, pp. 56–69, Feb. 2015.
- 1012 [14] L. Ruan, V. K. N. Lau, and M. Z. Win, "Generalized interference
1013 alignment—Part II: Application to wireless secrecy," *IEEE Trans. Signal*
1014 *Process.*, vol. 64, no. 10, pp. 2688–2701, May 2016.
- 1015 [15] M. Bloch and J. Barros, *Physical-Layer Security: From Information*
1016 *Theory to Security Engineering*. Cambridge, U.K.: Cambridge Univ.
1017 Press, 2011.
- 1018 [16] M. Z. Win, P. C. Pinto, and L. A. Shepp, "A mathematical theory of
1019 network interference and its applications," *Proc. IEEE*, vol. 97, no. 2,
1020 pp. 205–230, Feb. 2009.
- 1021 [17] A. Rabbachin, A. Conti, and M. Z. Win, "The role of aggregate interfer-
1022 ence on intrinsic network secrecy," in *Proc. Int. Conf. Commun. (ICC)*,
1023 Ottawa, ON, Canada, Jun. 2012, pp. 3548–3553.
- 1024 [18] K. I. Pedersen, P. E. Mogensen, and B. H. Fleury, "A stochastic model
1025 of the temporal and azimuthal dispersion seen at the base station in
1026 outdoor propagation environments," *IEEE Trans. Veh. Technol.*, vol. 49,
1027 no. 2, pp. 437–447, Mar. 2000.
- 1028 [19] H. Asplund, A. A. Glazunov, A. F. Molisch, K. I. Pedersen, and
1029 M. Steinbauer, "The COST 259 directional channel model—Part
1030 II: Macrocells," *IEEE Trans. Wireless Commun.*, vol. 5, no. 12,
1031 pp. 3434–3450, Dec. 2006.
- 1032 [20] J. Barros and M. R. D. Rodrigues, "Secrecy capacity of wireless
1033 channels," in *Proc. IEEE Int. Symp. Inf. Theory (ISIT)*, Jul. 2006,
1034 pp. 356–360.



1035 **Lorenzo Mucchi** (M'98–SM'12) received the
1036 Dr.Eng. (Laurea) degree in telecommunications
1037 engineering from the University of Florence, Italy,
1038 in 1998, and the Ph.D. degree in telecommunications
1039 and information society in 2001. Since 2001, he
1040 has been a Research Scientist with the Department
1041 of Information Engineering, University of Florence.
1042 In 2000, he spent a 12 month period of
1043 research at the Center for Wireless Communications,
1044 University of Oulu, Finland. He has been a Pro-
1045 fessor of information technologies with the Univer-
1046 sity of Florence, since 2008. His main research areas include theoretical
1047 modeling, algorithm design, and real measurements, mainly focusing on
1048 physical-layer security, visible light communications, ultra wideband tech-
1049 niques, localization, adaptive diversity techniques, and interference man-
1050 agement. He has authored or co-authored eight book chapters, 32 papers
1051 in international journals, and over 80 papers in international conference
1052 proceedings during his research activity. He was a member of the IEEE
1053 Communications and Information Security Technical Committee in 2009.
1054 Since 2016, he has been an Associate Editor of the IEEE COMMUNICATION
1055 LETTERS. In 2004, he was the Lead Organizer and the General Chair of
1056 the IEEE International Symposium on Medical ICT. He has been the Guest
1057 Editor and the Editor-in-chief of the Elsevier Academic Press Library. He was
1058 a member of the European Telecommunications Standard Institute Smart Body
1059 Area Network (SmartBAN) Group in 2013 and the Team Leader of the special
1060 task force 511 SmartBAN Performance and Coexistence Verification in 2016.



1061 **Luca Ronga** (S'89–M'94–SM'04) received the
1062 M.S. degree in electronic engineering and the Ph.D.
1063 degree in telecommunications from the University
1064 of Florence, Italy, in 1994 and 1998, respectively.
1065 In 1997, he joined as a Visiting Scientist
1066 the International Computer Science Institute of
1067 Berkeley, CA. In 1999, he joined Italian National
1068 Consortium for Telecommunications, where he is
1069 currently heads the research area. He has authored
1070 over 90 papers in international journals and confer-
1071 ence proceedings. His research interests span satel-
1072 lite communications to cognitive radio, software-defined radio, radio resource
1073 management, and wireless security. He has been an Editor of the *EURASIP*
1074 *Newsletter* for four years, a member of the ETSI SatEC Working Group, and
1075 a member of NATO Task Force on Cognitive Radio. He has been a principal
1076 investigator in several research projects.



1077 **Xiangyun Zhou** (M'11) received the Ph.D. degree
1078 from The Australian National University (ANU)
1079 in 2010. He is currently a Senior Lecturer with ANU.
1080 His research interests are in the fields of commu-
1081 nication theory and wireless networks. He was a
1082 recipient of the Best Paper Award at ICC in 2011
1083 and the IEEE ComSoc Asia-Pacific Outstanding
1084 Paper Award in 2016. He served as a Guest Editor
1085 of the *IEEE Communications Magazine* feature topic
1086 on wireless physical layer security in 2015. He has
1087 also served as the symposium, track, and workshop
1088 co-chair for major IEEE conferences. He was the Chair of the ACT Chap-
1089 ter of the IEEE Communications Society and Signal Processing Society
1090 from 2013 to 2014. He currently serves on the Editorial Board of the
1091 IEEE TRANSACTIONS ON WIRELESS COMMUNICATIONS and the IEEE
1092 COMMUNICATIONS LETTERS.



1093 **Kaibin Huang** (M'08–SM'13) received the B.Eng.
1094 degree (Hons.) and the M.Eng. degree from the
1095 National University of Singapore, and the Ph.D.
1096 degree from The University of Texas at Austin
1097 (UT Austin), all in electrical engineering. Since
1098 2014, he has been an Assistant Professor with the
1099 Department of Electrical and Electronic Engineer-
1100 ing (EEE), The University of Hong Kong. He was
1101 a Faculty Member with the Department of Applied
1102 Mathematics (AMA), The Hong Kong Polytechnic
1103 University (PolyU) and the Department of EEE,
1104 Yonsei University, South Korea, where he is currently an Adjunct Professor.
1105 He is also a University Visiting Scholar with Kansai University, Japan.
1106 His research interests focus on the analysis and design of wireless networks
1107 using stochastic geometry, and multi-antenna techniques. He received the
1108 2015 IEEE ComSoc Asia Pacific Outstanding Paper Award, the Outstanding
1109 Teaching Award from Yonsei, the Motorola Partnerships in Research Grant,
1110 the University Continuing Fellowship from UT Austin, and the Best Paper
1111 Award from the IEEE GLOBECOM 2006 and PolyU AMA in 2013. He
1112 frequently serves on the technical program committees of major IEEE
1113 conferences in wireless communications. Most recently, he served as the Lead
1114 Chair of the Wireless Communication Symposium of the IEEE Globecom
1115 2017 and the Communication Theory Symposium of the IEEE GLOBECOM
1116 2014 and the TPC Co-Chair of the IEEE PIMRC 2017 and the IEEE CTW
1117 2013. He was an Editor of the IEEE JOURNAL ON SELECTED AREAS
1118 IN COMMUNICATIONS Series on Green Communications and Networking
1119 from 2015 to 2016, the IEEE WIRELESS COMMUNICATIONS LETTERS
1120 from 2011 to 2016, and the IEEE/KICS JOURNAL OF COMMUNICATION
1121 AND NETWORKS from 2009 to 2015. He edited the IEEE JOURNAL ON
1122 SELECTED AREAS IN COMMUNICATIONS Special Issue on Communications
1123 Powered by Energy Harvesting in 2015. He was an elected member of the
1124 SPCOM Technical Committee of the IEEE Signal Processing Society from
1125 2012 to 2015. He is currently an Editor for the newly established IEEE
1126 TRANSACTIONS ON GREEN COMMUNICATIONS AND NETWORKING, and
1127 the IEEE TRANSACTIONS ON WIRELESS COMMUNICATIONS.



Yifan Chen (M'06–SM'14) received the B.Eng. (Hons.) and Ph.D. degrees in electrical and electronic engineering from Nanyang Technological University, Singapore, in 2002 and 2006, respectively. From 2005 to 2007, he was a Project Officer and then a Research Fellow with the Singapore-University of Washington Alliance in bio-engineering, supported by the Singapore Agency for Science, Technology and Research, Nanyang Technological University, Singapore, and the University of Washington at Seattle, WA, USA. From 2007 to

2012, he was a Lecturer and then a Senior Lecturer with the University of Greenwich and Newcastle University, U.K. From 2012 to 2016, he was a Professor and the Head of Department of Electrical and Electronic Engineering with the Southern University of Science and Technology, Shenzhen, China, appointed through the Recruitment Program of Global Experts (known as the Thousand Talents Plan). In 2013, he was a Visiting Professor with the Singapore University of Technology and Design, Singapore. He is currently a Professor of Engineering and the Associate Dean External Engagement with the Faculty of Science and Engineering and the Faculty of Computing and Mathematical Sciences, University of Waikato, Hamilton, New Zealand. His current research interests include electromagnetic medical imaging and diagnosis, transient communication with application to healthcare, touchable communication and computation with application to targeted drug delivery and contrast-enhanced medical imaging, fundamentals and applications of nanoscale and molecular communications, and channel modeling for next-generation wireless systems and networks. He is the Coordinator of the European FP7 CoNHealth Project on intelligent medical ICT, an elected Working Group Co-leader of the European COST Action TD1301 MiMed Project on microwave medical imaging, an Advisory Committee Member of the European Horizon 2020 CIRCLE Project on molecular communications, a Voting Member of the IEEE Standards Development Working Group 1906.1 on nanoscale and molecular communications, an Editor for the IEEE ComSoc Best Readings in Nanoscale Communication Networks and the IEEE Access Special Section in Nano-antennas, Nano-transceivers, and Nano-networks/Communications, and a Vice Chair of the IEEE Nano-scale, Molecular and Quantum Networking Emerging Technical Subcommittee.



Rui Wang received the bachelor's degree from the University of Science and Technology of China, in 2004, and the Ph.D. degree in wireless communications from The Hong Kong University of Science and Technology, in 2008. From 2009 to 2012, he was a Senior Research Engineer with Huawei Technologies, Co., Ltd. Since 2012, he has been with the South University of Science and Technology of China, as an Associate Professor. He has research experience in academia and industry. He has authored over 30 papers in top-level

IEEE journals and flagship international conferences, especially in the area of wireless radio resource optimization and interference management. He is also involved in the development of interference mitigation technology for 5G systems, and has contributed more than 20 U.S. patent applications and 40 Chinese patent applications (20 of them have been granted).

IEEE PROOF